S

Universitetet
i Stavanger

FACULTY OF SCIENCE AND TECHNOLOGY

MASTER'S THESIS

Study programme/specialisation: Petroleum Engineering - Well Engineering	Spring semester, 2017 Open
Author: Vebjørn Langåker	………………………………………… (signature of author)

Programme coordinator: Supervisor(s):   Dan Sui

Title of master's thesis: A temperature model for Extended Reach Drilling applications

Credits: 30 ECTS

Keywords: Temperature distribution, heat transfer, non-Newtonian behavior, energy source terms	Number of pages: 80 Stavanger,……………………….

Acknowledgements

Abstract

Ensuring precise estimation of temperature is a critical process for well planning and real-time drilling operations, especially for Extended Reach Drilling (ERD). Therefore, a temperature model has been developed to predict accurate wellbore temperature distributions for ERD applications. The model offers improvements to existing circulating temperature models in terms of more realistic drilling fluid properties and by introducing effects of heat sources that occurs in a drilling operation.

In this work, temperature dependent drilling fluid transport and thermal properties are considered to improve the accuracy of the temperature model. Experiments have been performed to determine the behavior of drilling fluid density and viscosity under high pressure and high temperature conditions. Measurements of viscosity allows the effect of non-Newtonian behavior to be included in the convective heat transfer processes. Furthermore, applying a non-Newtonian pressure loss model enables an opportunity to incorporate the impact of non-Newtonian behavior on the wellbore pressure distribution and thus pressure dependent drilling fluid properties. Another important aspect of the approach in this work, is the introduction of heat source terms. Heat generation that occurs during drilling processes have the potential to affect the wellbore temperature distribution. To give a better estimation of wellbore heat transfer processes, heat generation due to drill pipe rotation, drill bit friction, frictional pressure losses, and the Joule-Thomson coefficient is considered.

Results from a sensitivity analysis indicate that parameters related to the hydraulics of a wellbore system have a significant effect on the temperature distribution. The flow rate is found to be a major contributor. Drilling fluid viscosity, density, and specific heat capacity have also shown significant effect on the temperature distribution. On the other hand, mechanical processes and heat generation due to friction are found to be less dominant. Results verify that the approach in this thesis provides an accurate wellbore temperature distribution with the possibility to enhance drilling performance and optimize well design.

Contents

1 Introduction

Extended Reach Drilling (ERD) is a term that involves wells with large horizontal displacements. By definition, a well with a horizontal displacement to true vertical depth ratio of 2 or higher is regarded as an ERD well. Note that horizontal displacement in this case is measured from the kick off point (Rubiandini R.S, 2008). ERD wells emerged in the early 1990's as technology were improved to achieve optimized and cost efficient solutions. The improvement of technology was necessary to access reserves that previously were not economically or technically feasible to produce. This gave an opportunity to extend the life of mature fields and to optimize field development through a reduction of drilling sites and structures (Payne, Cocking, & Hatch, 1994). Furthermore, ERD designs gives the ability to increase the drainage capability of a reservoir by installing horizontal completions over large sections. Examples of challenging and successful ERD designs are found in for example the Wytch Farms project (BP) and the Sakhalin-1 project (Exxon Neftegas Limited).

Compared to a conventional design, ERD wells will often have longer sections of higher inclinations. An ERD design results in challenges that are less pronounced in the conventional design. For example, torque and drag related issues tend to be more severe in ERD wells. In a long and highly deviated section, a large part of the drill pipe weight will lay on the low side of the wellbore and consequently increase the frictional forces. Torque and drag may become a limiting factor as the frictional forces increases. Problems related to excessive torque and drag are buckling behavior, insufficient WOB, and inability to reach target. Another issue that increases in complexity with wellbore length and inclination, is hole cleaning. The effect of annular velocity on cuttings transport diminishes with increasing inclination. Cuttings will therefore settle easier and cuttings beds may form. Moreover, the cuttings beds tend to slide downwards in the wellbore as avalanches for inclinations of 30-60 degrees (Tomren, Iyoho, & Azar, 1986). Insufficient hole cleaning has the potential to cause pipe sticking, reduction of ROP, excessive torque and drag, and more. Drilling fluid design is also a factor that is critical for ERD wells. Controlling drilling fluid properties can be an issue for deep and long wells, and problems related to borehole stability, lost circulation, barite sag, ECD management, torque and drag, and hole cleaning can occur (Cameron, 2001).

Another important aspect of ERD is wellbore temperature. Drilling further and deeper comes with an increased formation temperature, and it is not unusual that ERD wells are exposed to HPHT conditions. High temperatures have the potential to cause severe operational problems. For example, increasing the temperature will affect the ability of the drilling fluid to maintain its properties and thus ensure well control and avoid the problems listed above. Additionally, high temperatures can be a limiting factor for downhole drilling tools and the ability to perform directional control and logging. It is consequently critical to provide realistic estimations of wellbore temperatures. Therefore, the objective of this thesis is to develop a sophisticated temperature model that can predict accurate wellbore temperature distributions for ERD applications.

The approach and related theory to the development of the model is explained in chapter 2. Energy source terms that occurs during drilling operations are implemented to improve existing circulation models and to give a more realistic representation of the wellbore temperature distribution. The considered source terms are heat generation due to drill pipe rotation, drill bit friction, frictional pressure losses and the effect of the Joule-Thomson coefficient. Furthermore, a sensitivity analysis and discussion of the results are given in chapter 3. The sensitivity analysis includes parameters such as wellbore design, drilling fluid transport and thermal properties, formation temperature and thermal properties, and the energy source terms. Determining how these parameters affect the wellbore temperature distribution has the potential to enhance drilling performance and provide optimized designs for ERD wells.

2 Temperature model and supporting theory

2.1 Wellbore heat transfer

For a drilling scenario, temperature differences between the wellbore and the formation result in a transfer of thermal energy. Heat may flow from formation to wellbore or vice versa depending on the relative temperatures. For example, if the formation temperature is higher than the temperature of the wellbore at a certain depth, the wellbore system will gain energy in terms of heat. By nature, heat will continue to flow from the formation to the wellbore until a thermal equilibrium is reached.

Formation temperature can in a large scale be represented by a function of depth. As a well is drilled into the crust of the Earth, it approaches warmer areas and a general temperature increase is observed. The rate at which the temperature increases is expressed in terms of the geothermal gradient. The geothermal gradient is a governing factor for the wellbore temperature distribution. Therefore, an accurate estimation is critical for well planning, especially for ERD and HPHT wells where temperature may become a limiting factor. Determining an accurate geothermal gradient becomes a challenge in some cases as the gradient is location-specific and may vary between both regions and oil fields. Forrest, Marcucci, and Scott (2005) mapped and calculated geothermal gradients for 1131 fields and wells in the northern Gulf of Mexico. Results reveal significant variation from region to region and indicate a complex pattern of subsurface heat. To meet this challenge, geothermal gradients are often based on data from nearby wells. In chapter 3.8, a sensitivity analysis of the geothermal gradient and its impact on the wellbore temperature distribution is given to emphasize the importance of a representative estimation.

The amount of heat flowing to or from the wellbore is also sensitive to wellbore design and drilling parameters. Consider the general wellbore schematic shown in figure 2-1. In the first section, drilling fluid enters the drill pipe at a known temperature. As the fluid flows down the pipe, its temperature will change due to heat transfer processes with its surroundings and through heat generation from energy sources present in the drill pipe. More specifically, the vertical temperature distribution throughout the drill pipe is a result of (Santoyo-Gutiérrez, 1997):

- the convective heat transfer within the fluid column
- the rate of convective heat transfer between the fluid, the drill pipe wall, and the annular fluid
- heat generation from fluid friction

Picture an arbitrary point in the wellbore where the annulus temperature exceeds that of the drill pipe. Because of the temperature difference, a convective heat transfer occurs between the moving annulus fluid and the outer surface of the drill pipe. When the outer wall of the drill pipe is heated up, heat is transferred through the thickness of the pipe wall via conduction to the relatively cooler inner wall. The heat is further transferred via convection between the surface of the pipe wall and the moving drill pipe fluid, resulting in a temperature increase at that reference point. Note that vertical conduction is also present in the fluid column. However, forced convection is the dominant process during circulation and conduction within the fluid is normally neglected. This is a reasonable assumption adopted by for example Raymond (1969), Marshall and Bentsen (1982), and Santoyo-Gutiérrez (1997).

Section 2 in the illustration below, represents the drill bit. The length of this section is negligible compared to the length of the wellbore, and section 2 is accordingly considered as a single point. Still, heat generated at this point will have an impact on the wellbore temperature distribution. One of the energy sources present is the frictional pressure losses across the bit. Compared to the annular pressure losses, the bit pressure loss typically accounts for a larger portion of the total pressure losses throughout the wellbore (Warren, 1989; Aadnøy, 2010). Thus, heat generation due to fluid friction is greater at the bit than for the entire annulus section. Another energy source at Section 2 is the heat generation from frictional forces between the bit and the formation during drilling. It appears to be a lack of studies regarding the actual amount of energy released during this process. Keller, Couch, and Berry (1973) proposed that the total mechanical energy input required to rotate the drill pipe is converted to heat and that 40% of it is necessary to cut the rock. Corre, Eymard, and Guenot (1984) on the other hand, suggested that about 10% was sufficient.

After the drilling fluid has passed through the bit, it enters section 3, namely the annulus. As the fluid flows up the annulus, the vertical temperature distribution is affected by (Santoyo-Gutiérrez, 1997):

4

- the convective heat transfer within the fluid column
- the rate convective heat transfer between the fluid, the drill pipe wall, and the drill pipe fluid
- the convective heat transfer between the annulus fluid, any layers of casing and cement or fluid, and the formation
- the conductive heat transfer from the formation
- heat generation related to fluid friction and drill pipe rotation and movement

Consider the location of point 3 in figure 2-1. Given that the formation temperature exceeds the wellbore temperature, heat will transfer via conduction from the formation and through the cement and casing. In the annulus, heat is transferred from the casing wall to the moving fluid by convection. Heat continues to flow up the annulus by convection within the fluid itself, and heat is lost to the drill pipe section by the processes described in the fourth paragraph in this chapter, if the temperature in the annulus is greater than the drill pipe temperature.

As discussed, the wellbore temperature distribution is affected by formation temperature and heat conduction from the formation. To ensure an accurate estimation of these parameters, many authors have conducted investigations regarding formation temperature distribution and rate of heat transfer. A common approach is to consider a transient and radial heat conduction. Ramey (1962) evaluated the application of different solutions for radial heat conduction from an infinite long cylinder and gave recommended models for wellbore heat transfer applications. Chiu and Thakur (1991) have also presented and discussed the application of several models for transient heat loss in the formation. In this thesis, the approach from Hasan and Kabir (1991) is implemented. Hasan and Kabir (1991) presented a rigorous solution for the formation heat loss and improved the existing approaches recommended by Ramey (1962) by including Fourier's law of heat conduction as a boundary for the formation/wellbore interface. Acknowledging that the solution would not be efficient in computer programs due to its complexity, an algebraic approximation was also given. The algebraic solution is based on trends in the results from the rigorous solution, and it is given by:

$$T_D = 1.1281\sqrt{t_d}\left(1 - 0.3\sqrt{t_d}\right) \text{ for } t_d \leq 1.5 \tag{2.1}$$

$$T_D = [0.4036 + 0.5\ln(t_d)]\left[1 + \frac{0.6}{t_d}\right] \quad \text{for } t_d > 1.5 \tag{2.2}$$

where

$$t_d = \frac{\alpha t}{r_{wb}^2}$$

and

$$\alpha = \frac{k_f}{c_{pf}\rho_f}$$

Here, T_D represents the dimensionless temperature and t_d represents the dimensionless time as defined in Hasan and Kabir (1991). The dimensionless temperature gives the transient behavior of the formation temperature, and depending on the dimensionless time, equations (2.1) and (2.2) are applied in this thesis to derive a solution for and determine the wellbore temperature distribution.
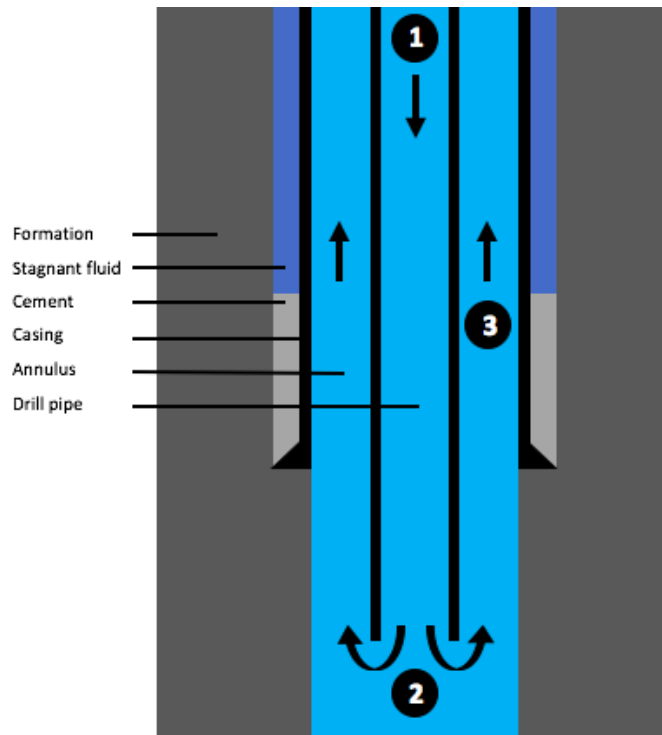

Figure 2-1 Wellbore schematic

Nomenclature

c_{pf}: formation specific heat capacity, J/kg°C
k_f: formation conductivity, W/m°C
r_{wb}: wellbore radius, m
t: time, s
T_D: dimensionless temperature
t_D: dimensionless time
α: formation heat diffusivity, m²/s
ρ_f: formation density, kg/m³

2.2 Transport and thermophysical properties of drilling fluid

2.2.1 Convective heat transfer coefficient

Convection is defined as the heat transfer that occurs between a surface and a moving fluid at different temperatures (Bergman, Incropera, DeWitt, & Lavine, 2011). Simply put, a drilling operation involves pumping a fluid through a circular conduit. If the fluid and the surface of the conduit have different temperatures, a convective heat transfer will occur. More specifically, convection is a combination of two mechanisms (Bergman et al., 2011). Energy is transferred by both diffusion and the bulk motion of the fluid. Close to the wall of a conduit, fluid velocity approaches zero and diffusion (conduction) dominates the heat transfer. Here, heat is transferred from the wall surface to the nearby fluid layer by random molecular motion. The heat going into this layer is transferred further away from the wall by the bulk motion of the fluid, and into the high velocity region. The expression for the convective heat transfer process is given by Newton's law of cooling:

$$q'' = h(T_s - T_m) \qquad (2.3)$$

where h is the convective heat transfer coefficient (CHTC), and T_s and T_m represent the temperature of the conduit surface and the mean temperature of the fluid, respectively.

In chapter 2.1, the heat transfer processes that occur in a wellbore is discussed. It was mentioned that there exists a convective heat transfer between the drill pipe fluid, the drill pipe wall, and the annulus fluid. The same process occurs between the annulus fluid, the casing wall and a possible cement layer, and the formation. Instead of applying equation (2.3) to describe these processes individually, an overall heat transfer coefficient that considers the net resistance of heat flow over several layers, is used. The convective heat transfer is modeled by the following equations (Kabir, Hasan, Kouba, & Ameen, 1996):

$$Q_{ap} = 2\pi r_{pi} U_p (T_a - T_p) dx \qquad (2.4)$$

$$Q_{wa} = 2\pi r_{ci} U_a (T_w - T_a) dx \qquad (2.5)$$

where Q_{ap} and Q_{wa} represents the overall rate of heat transfer from the annulus to the drill pipe and from the formation/wellbore interface to the annulus, respectively. The overall heat transfer coefficient is denoted by U. Thompson and Burgess (1985) defined U_p and U_a as

$$\frac{1}{U_p} = \frac{1}{h_p} + \frac{r_{pi}}{r_{po}}\frac{1}{h_a} + \frac{r_{pi}}{k_p}\ln\left(\frac{r_{po}}{r_{pi}}\right)$$
(2.6)

$$\frac{1}{U_a} = \frac{1}{h_a} + \frac{r_{ci}}{k_c}\ln\left(\frac{r_{co}}{r_{ci}}\right) + \frac{r_{ci}}{k_{cement}}\ln\left(\frac{r_w}{r_{c0}}\right)$$
(2.7)

For equation (2.7), it is possible to include additional casing strings and cement layers.

Inspecting the equations above reveals that the CHTC plays an important role for the heat rate and thus the wellbore temperature distribution. The CHTC in pipe flow is determined by the dimensionless Nusselt number given below:

$$Nu = \frac{hD}{k}$$
(2.8)

where k is the conductivity of the fluid and D is the pipe diameter. The Nusselt number gives a relationship between the convective and the conductive heat transfer, and a large Nusselt number indicates an efficient convection process. For laminar flow, the Nusselt number takes a constant value of

$$Nu = 4.36$$
(2.9)

with the assumption of a uniform wall heat flux (Bergman et al., 2011; Rohsenow, Hartnett, & Cho, 1998). Estimating the Nusselt number for turbulent flow is more complex. Research show that the CHTC becomes a complicated function of fluid properties and flow geometry (Santoyo, Garcia, Espinosa, Santoyo-Gutiérrez, & González-Partida, 2003). It is therefore common to use correlations to estimate the Nusselt number for turbulent flow. Many researchers have presented work on this subject. A summary of the most common correlations is for example given in the work by (Santoyo et al., 2003). In this thesis, the well-known Dittus-Boelter correlation is applied to estimate the CHTC. The Dittus-Boelter equation gives the Nusselt number as a function of Reynolds number and Prandtl number:

$$Nu = 0.023Re^{0.8}Pr^n \tag{2.10}$$

where n is set to 0.3 for cooling processes and 0.4 for heating processes. Equation (2.10) is valid for:

$$0.7 \leq Pr \leq 160$$

$$10\,000 \leq Re$$

$$10 \leq \frac{L}{D}$$

And Reynolds number and Prandtl number are defined as

$$Re = \frac{\rho v D}{\mu} \tag{2.11}$$

$$Pr = \frac{c_p \mu}{k} \tag{2.12}$$

Now, it is possible to express the CHTC as

$$h = 0.023 \left(\frac{\rho v D}{\mu}\right)^{0.8} \left(\frac{c_p \mu}{k}\right)^n \frac{k}{D} \tag{2.13}$$

Equation (2.13) provides valuable information about which parameters that control the CHTC and thus affect the wellbore temperature distribution. It is especially of interest to determine to what extent drilling fluid transport and thermal properties impact heat transfer processes in a wellbore system. A sensitivity analysis of the parameters in equation (2.13) is presented in chapter 3, and the models for drilling fluid density and viscosity is discussed further in the next chapters.

c_p: fluid specific heat capacity, kg/J°C

D: pipe diameter, m

h: convective heat transfer coefficient, W/m²°C

k: fluid thermal conductivity, W/m°C

L: pipe length, m

Nu: Nusselt number

Q: heat rate, J/s

q'': heat flux, W/m²

r_{ci}: casing inner radius, m

r_{co}: casing outer radius, m

r_{pi}: drill pipe inner radius, m

r_{po}: drill pipe outer radius, m

T: temperature, °C

U: overall heat transfer coefficient, W/m²°C

v: fluid velocity, m/s

ρ: fluid density, kg/m³

μ: fluid viscosity, Pas

Subscripts

a: annulus

c: casing

m: mean

p: pipe

s: conduit surface

w: wellbore

2.2.2 Density model

Drilling fluid is a critical factor for drilling operations. Some of the most important functions of drilling fluids are to ensure borehole stability and well control. These functions are maintained through controlling the wellbore pressure and thus the drilling fluid density. Consequently, the drilling fluid density impacts the ability to ensure borehole stability and well control, and it becomes important to give accurate estimations of the density. Density of a drilling fluid varies with pressure and temperature. An increase of pressure will compress the drilling fluid and result in an increase of density. Increasing the temperature on the other hand, expands the drilling fluid and decreases the density. The wellbore temperature distribution will therefore affect critical functions of the drilling fluid. Variation in density with temperature and pressure are well-known effects, and the intention in this work is instead to investigate the effect density has on heat transfer processes.

Take equation (2.13) as an example. It is evident that the CHTC and correspondingly the rate of convective heat transfer, is affected by density changes. The density will further affect the CHTC because of the pressure dependency of viscosity. In this thesis, the effect of drill pipe rotation as an energy source is discussed in chapter 2.4.1. The amount of generated heat from rotational effects are influenced by buoyancy forces and ultimately the drilling fluid density. These examples are mentioned to highlight that the effect of density on the wellbore temperature is complicated. Furthermore, as the density impacts heat transfer processes and the wellbore temperature, it will impose changes on itself through its variation with temperature, resulting in a coupled effect. It is therefore necessary to understand both how the density changes with temperature and the effects it has on the temperature distribution.

The linearized equation of state as shown below, is applied to determine the density behavior with varying pressure and temperature (Stamnes, 2011).

$$\rho = \rho_0 + \frac{\rho_0}{\beta}(P - P_0) - \rho_0 \alpha (T - T_0) \tag{2.14}$$

Here, ρ_0, P_0, and T_0 represents the density, pressure, and temperature at the point of linearization. The cubical expansion coefficient and the isothermal bulk modulus of the drilling fluid is given by α and β respectively. Stamnes (2011) state that the model is applicable for most drilling fluid for pressures and temperatures in the range of

$$0 < P < 500 \; bar$$

$$0 < T < 200 \; °C$$

In this thesis, the cubical expansion coefficient and the isothermal bulk modulus have been determined through a regression analysis of PVT data for an OBM. The results from the regression analysis and the linearization points of the conducted experiment are given in table 2-1. Figure 2-2 shows the variation in density with pressure and a selection of temperatures for the considered OBM.
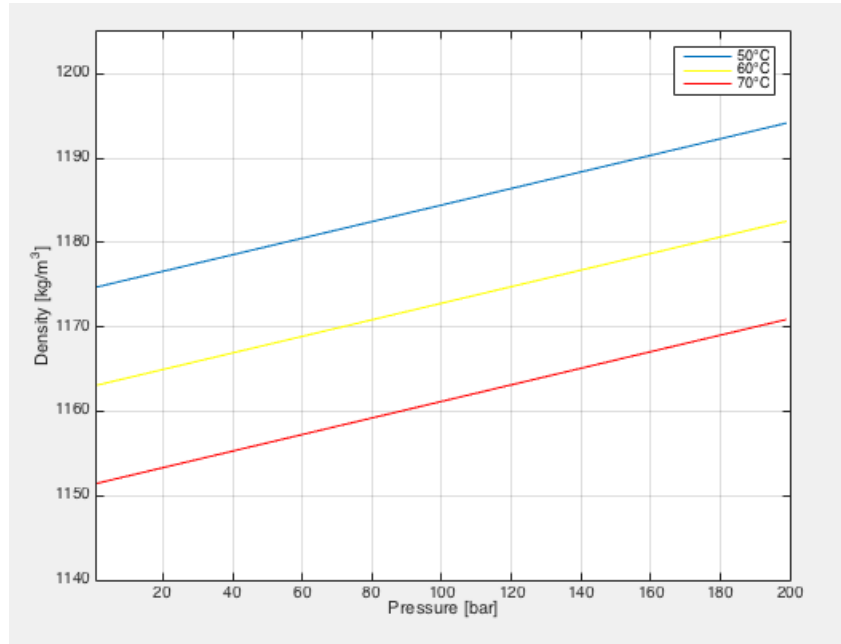
Figure 2-2 Density behavior of the considered OBM

$\boldsymbol{\alpha}$	$9.658 * 10^{-4}$	1/°C
$\boldsymbol{\beta}$	$8.146 * 10^{10}$	Pa
$\boldsymbol{\rho_0}$	1205	kg/m^3
$\boldsymbol{P_0}$	10^5	Pa
$\boldsymbol{T_0}$	24	°C

Table 2-1 Experimental values for the linearized equation of state

Nomenclature

P: pressure, Pa
T: temperature, °C
α: cubical expansion coefficient, 1/°C
β: isothermal bulk modulus, Pa
ρ: drilling fluid density, kg/m^3

2.2.3 Non-Newtonian viscosity

Viscosity is a key parameter to consider when determining fluid rheology and how it affects the rate of heat transfer in the wellbore. Drilling fluid viscosity is a function pressure, temperature, and composition. At increasing pressures and isothermal conditions, a general trend of increased viscosity is observed, and increasing the temperature during isobaric

conditions results in a decrease of the viscosity (Poling, Prausnitz, & O'connell, 2001). It is therefore important to include pressure and temperature dependent viscosity behavior to determine the effect of viscosity on wellbore heat transfer. Another factor to consider is the non-Newtonian nature of drilling fluids. Santoyo et al. (2003) report that temperature dependent viscosities of Newtonian and non-Newtonian fluids differ significantly. Using a Newtonian viscosity model for drilling fluids in a temperature model will overestimate the CHTC and the rate of heat transfer in the wellbore.

To include the factors mentioned above, rheology data of the OBM referred to in chapter 2.2.2. is implemented in this work. A high pressure high temperature rheometer was used to determine the rheological behavior of the drilling fluid for a pressure and temperature range of 40-160 bar and 25-80 °C respectively. The results are used in the temperature model to apply the correct viscosity according to the pressure and temperature variation throughout the wellbore. Analyzing the rheology data showed that a Herschel-Bulkley model provided the best fit overall. An example of that is given in figure 2-3, where the shear rate versus shear stress for the OBM at a pressure of 40 bar and temperature of 50 °C, is compared to estimated values by the Herschel-Bulkley model. The general Herschel-Bulkley model is given by equation (2.15) (Fan, Zhou, Wang, Peng, & Wang, 2014):

$$\tau = \tau_0 + K\gamma^n$$
(2.15)

and the parameters for the example in figure 2-3 are provided in table 2-2.

The apparent viscosity of a HB-fluid can be determined by the following model:

$$\mu_{app} = \frac{\tau}{\gamma} = \tau_0\gamma^{-1} + K\gamma^{n-1}$$
(2.16)

Unlike Newtonian fluid, the apparent viscosity of a non-Newtonian fluid depends on the shear rate and thus the flow rate. A relation between flow rate and rheological behavior is consequently necessary to determine the corresponding apparent viscosity and include the effect of non-Newtonian behavior on the heat transfer. In chapter 2.3.1, a pressure loss model for Herschel-Bulkley fluids is presented. This model includes a relation between wall shear

stress and flow rate that is taken advantage of to obtain the apparent viscosity. More details about this approach is given in the respective chapter.
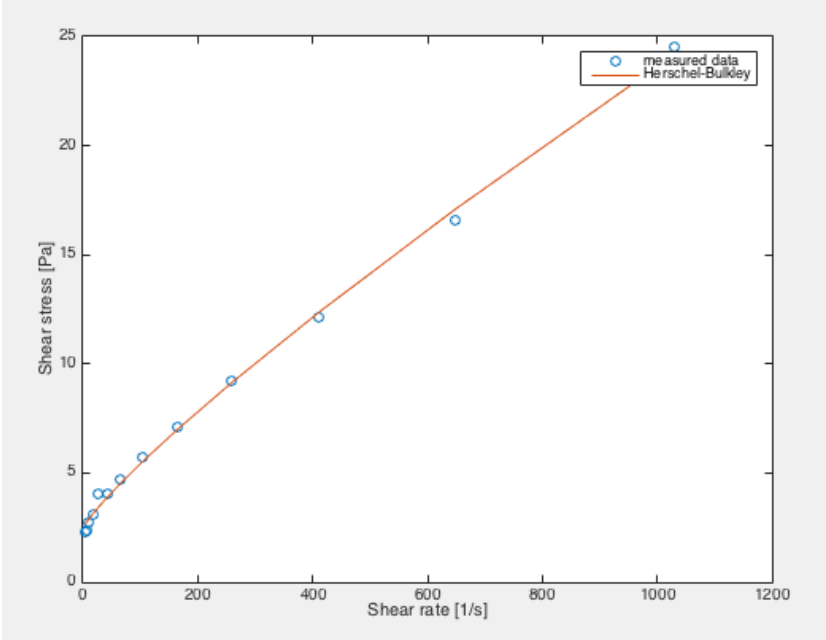

Figure 2-3 Comparison of experimental values with the Herschel-Bulkley model

τ_0	2.4689	Pa
K	0.0577	Pas^n
n	0.8549	-

Table 2-2 Experimental Herschel-Bulkley parameters

Nomenclature

K: consistency index, Pas^n
n: flow index
γ: shear rate, s^{-1}
τ: shear stress, Pa
τ_0: yield stress, Pa

2.3 Pressure losses

As discussed in chapters 2.2.2. and 2.2.3., thermal properties of drilling fluids are sensitive to transport properties such as density and viscosity. It was also suggested that the effect of non-Newtonian behavior on viscosity should not be ignored. The transport properties are functions of both pressure and temperature and pressure loss calculations will ultimately influence the thermal properties and the accuracy of the temperature distribution. Additionally, the pressure losses through a wellbore serves as an energy source which add heat to the system. It is therefore important to choose an appropriate pressure loss model. To ensure a representative estimation of the pressure losses and to obtain the apparent viscosity, a model that considers non-Newtonian effects for both the drill pipe the and annulus is implemented in this thesis. Furthermore, a model for bit pressure loss that includes an optimized nozzle discharge coefficient for roller cone bits, is applied and presented in chapter 2.3.2.

2.3.1 Non-Newtonian pressure loss

There are many authors that have published articles addressing the topic of non-Newtonian flow and frictional pressure losses. One of the most cited articles related to this subject is a study by Metzner and Reed (1955). They performed experiments with Power Law fluids and defined how the friction factor varies with Reynolds number for laminar, transitional, and turbulent flow. Four decades later, Reed and Pilehvari (1993) presented an analytical procedure for the determination of frictional pressure losses for Power Law, Bingham Plastic, and Herschel-Bulkley fluids based on the work of Metzner and Reed (1955). A more recent study by Fan et al. (2014) that provides a hydraulic model for Herschel-Bulkley fluids, is adopted in this thesis. It follows the same approach as Reed and Pilehvari (1993), but with a new definition of an effective diameter for annular flow. The basic idea behind this approach is to utilize established equations for Newtonian pipe flow to model non-Newtonian flow in both pipes and concentric annuli. Introducing a generalized effective diameter enables classical relations for Newtonian pipe flow to apply for non-Newtonian fluids and annular geometry. Fan et al. (2014) successfully validated their model by comparing results with measurements obtained from experimental data and field cases. The model is presented below.

Flow rate

Pipe flow

For steady-state laminar flow of time-independent viscous fluids in pipes, flow rate is related to wall shear stress by the following equation:

$$Q = \frac{\pi R^3}{\tau_w^3} \int_0^{\tau_w} \tau^2 \gamma d\tau \qquad (2.17)$$

This is a general expression for viscous fluids, which may be extended to include yield stress fluids and non-Newtonian behavior by integrating over the interval $[\tau_0, \tau_w]$.

$$Q = \frac{\pi R^3}{\tau_w^3} \int_{\tau_0}^{\tau_w} \tau^2 \gamma d\tau s \qquad (2.18)$$

Combining equation (2.15) with (2.18) and integrating, gives a relationship for pipe flow rate and wall shear stress for Herschel-Bulkley fluids as shown below.

$$Q_p = \frac{n\pi R^3}{3n+1}\left(\frac{\tau_w}{K}\right)^{\frac{1}{n}}\left(1 - \frac{\tau_0}{\tau_w}\right)^{\frac{n+1}{n}}\left[1 + \frac{2n}{2n+1}\left(\frac{\tau_0}{\tau_w}\right) + \frac{2n^2}{(n+1)(2n+1)}\left(\frac{\tau_0}{\tau_w}\right)^2\right] \qquad (2.19)$$

Annular flow

To derive the relationship between flow rate and shear stress for annular flow, a slot model is applied. In this approach, two thin ring elements with a thickness *dr* and radii of *(R0+Ri)/2+r* and *(R0+Ri)/2-r* are considered and used in the derivations. The flow rate is given as

$$Q = \int_0^{\frac{R_\delta}{2}} 2\pi(R_0 + R_i)u dr = 2\pi(R_0 + R_i)\left(ur|_0^{\frac{R_\delta}{2}} - \int_0^{\frac{R_\delta}{2}} r\frac{du}{dr} dr\right) \qquad (2.20)$$

where *u* is the velocity evaluated at a distance *r* from the center of the annular segment and the annular clearance is defined as

$$R_\delta = R_0 - R_i \qquad (2.21)$$

At the annulus wall where r is equal to $R_\delta/2$, the velocity becomes zero with the assumption of no slip at the wall. Consequently, the first term inside the last bracket of equation (2.20) also becomes zero and equation (2.20) simplifies to:

$$Q = 2\pi(R_0 + R_i)\left(\int_{\frac{\delta}{2}}^{\frac{R_\delta}{2}} r\left(-\frac{du}{dr}\right) dr\right) \tag{2.22}$$

where *du/dr* represents the shear rate. Here, the integration interval is updated to account for yield stress fluids at which the shear rate is zero when r is less than *δ/2*. Equation (2.23) gives the shear stress of a fluid at position *r*.

$$\tau = \frac{\Delta P r}{L} \tag{2.23}$$

The shear stress at the annular wall can be expressed in a similar manner by the introduction of a hydraulic diameter D_h as shown below.

$$\tau_w = \frac{\Delta P D_h}{4L} = \frac{\Delta P R_\delta}{2L} \tag{2.24}$$

where

$$D_h = D_0 - D_i \tag{2.25}$$

Dividing equation (2.23) by (2.24) yields:

$$\frac{\tau}{\tau_w} = \frac{2r}{R_\delta} \tag{2.26}$$

Reorganizing equation (2.26) and applying differentials give the two following expressions:

$$r = \frac{R_\delta}{2\tau_w}\tau \tag{2.27}$$

$$dr = \frac{R_\delta}{2\tau_w}d\tau \tag{2.28}$$

Furthermore, by using the fact that shear rate is a function of shear stress and implementing equations (2.27) and (2.28) to equation (2.22), the flow rate may be expressed as

$$Q = \frac{\pi(R_0 + R_i){R_\delta}^2}{2{\tau_w}^2} \int_{\tau_0}^{\tau_w} \tau \gamma \, d\tau \tag{2.29}$$

Finally, annular flow rate for a Herschel-Bulkley fluid is obtained by inserting equation (2.15) into equation (2.29) and integrating over the given interval.

$$Q_a = \frac{n\pi {R_\delta}^2}{2(2n+1){\tau_w}^2 K^{\frac{1}{n}}}(R_0 + R_i)(\tau_w - \tau_0)^{\frac{n+1}{n}}\left(\tau_w + \frac{n}{n+1}\tau_0\right) \tag{2.30}$$

Generalized flow index

Metzner and Reed (1955) developed a method of extending their results for Power Fluids to account for all time-independent, non-Newtonian fluids by defining the generalized flow index shown below.

$$n' = \frac{d \ln \tau_w}{d \ln \left(\frac{8v}{D}\right)} \tag{2.31}$$

They also gave a generalized expression for the wall shear rate.

$$\gamma_w = \frac{3n' + 1}{4n'}\left(\frac{8v}{D}\right) \tag{2.32}$$

For comparison, the wall shear rate for Newtonian pipe flow is given in equation (2.33).

$$\gamma_{w,N} = \frac{8v}{D} \tag{2.33}$$

Note that in the model by Fan et al. (2014), n' represents the general flow index for a Herschel-Bulkley fluid.

Pipe flow

For pipe flow, equations (2.31) and (2.32) are given as

$$n_p{}' = \frac{d \ln \tau_w}{d \ln \left(\frac{8v}{D}\right)}$$

(2.34)

$$\gamma_{w,p} = \frac{3n_p{}' + 1}{4n_p{}'} \left(\frac{8v}{D}\right)$$

(2.35)

Annular flow

With respect to annular flow, Fan et al. (2014) employs an approach that deviates slightly from that of Reed and Pilehvari (1993). First, they present the Newtonian wall shear rate for a concentric annulus.

$$\gamma_{w,a,N} = \frac{12v}{D_h}$$

(2.36)

This equation is rearranged to put it in the same form as for pipe flow.

$$\gamma_{w,a} = \frac{8v}{\frac{2}{3}D_h}$$

(2.37)

Here, Fan et al. (2014) use a relation for annular flow rate as given in (2.38) and combine it with equation (2.29) to produce equation (2.39).

$$Q_a = \pi(R_0 + R_i)R_\delta v$$

(2.38)

$$\frac{8v}{\frac{2}{3}D_h} \tau_w{}^2 = 3 \int_{\tau_0}^{\tau_w} \tau \gamma d\tau$$

(2.39)

Moreover, equation (2.39) is restructured and given on the following form:

(2.40)

$$\gamma_{w,a} = \frac{2}{3}\left(\frac{8v}{\frac{2}{3}D_h}\right) + \frac{1}{3}\frac{d\left(\frac{8v}{\frac{2}{3}D_h}\right)}{d\tau_w}\tau_w$$

From the latter equation, an expression for the generalized flow index in annuli is derived.

$$n_a' = \frac{d\ln\tau_w}{d\ln\left(\frac{8v}{\frac{2}{3}D_h}\right)} \tag{2.41}$$

And finally, the expression for a generalized annulus wall shear stress becomes:

$$\gamma_{w,a} = \frac{2n_a' + 1}{3n_a'}\left(\frac{8v}{\frac{2}{3}D_h}\right) \tag{2.42}$$

Generalized effective diameter

As mentioned previously, applying a generalized effective diameter provides the opportunity to determine non-Newtonian pressure loss using established analytical models for Newtonian pipe flow. From equations (2.35) and (2.42) the effective diameter is defined as

$$D_{eff,p} = \frac{4n_p'}{3n_p' + 1}D \tag{2.43}$$

$$D_{eff,a} = \frac{2n_a'}{2n_a' + 1}D_h \tag{2.44}$$

Now, the wall shear rate for non-Newtonian flow may be expressed in the same form as for Newtonian pipe flow given in equation (2.33).

$$\gamma_w = \frac{8v}{D_{eff}} \tag{2.45}$$

Additionally, the Reynolds number is also generalized to account for any non-Newtonian fluid by introducing the effective diameter as shown below.

20

$$Re_g = \frac{\rho D_{eff} v}{\mu_{w,app}} \qquad (2.46)$$

For a Herschel-Bulkley fluid, the apparent viscosity at the wall is given by equation (2.47) and the generalized Reynolds number for pipes and annuli is given by equation (2.48) and (2.49) respectively.

$$\mu_{w,app} = \frac{\tau_w}{\gamma_w} = \tau_0 \gamma_w^{-1} + K \gamma_w^{n-1} \qquad (2.47)$$

$$Re_{g,p} = \frac{\rho \left(\dfrac{4n_p{}'}{3n_p{}' + 1} \right) Dv}{\mu_{w,app}} \qquad (2.48)$$

$$Re_{g,a} = \frac{\rho \left(\dfrac{2n_a{}'}{2n_a{}' + 1} \right) D_h v}{\mu_{w,app}} \qquad (2.49)$$

Friction factor

The generalized Reynolds number is applied to the fanning friction factor to determine the pressure drop of laminar flow.

$$f = \frac{64}{Re_g} \qquad (2.50)$$

For transitional and turbulent flow, the friction factor is obtained by equation (2.51), which is a modified version of Colebrook's equation that is valid for any time-independent fluids flowing through pipes and concentric annuli.

$$\frac{1}{\sqrt{f}} = -4 \log_{10} \left[\frac{0.27\varepsilon}{D_{eff}} + \frac{1.26^{(n')^{-1.2}}}{\left[Re_g f^{(1-0.5n')} \right]^{(n')^{-0.75}}} \right] \qquad (2.51)$$

Pressure loss

The expressions for pressure loss for pipe and annular flow are given by equations (2.52) and (2.53).

$$\frac{dP}{dL_p} = \frac{f \, \rho v^2}{2D} \tag{2.52}$$

$$\frac{dP}{dL_a} = \frac{f \, \rho v^2}{2D_h} \tag{2.53}$$

Finally, the apparent viscosity and the pressure drop for a Herschel-Bulkley fluids can be computed by following the procedures given below.

Pipe flow

1. Give the flow rate and solve equation (2.19) to obtain the wall shear stress $\tau_{w,p}$
2. Use $\tau_{w,p}$ in equation (2.15) and solve for the wall shear rate $\gamma_{w,p}$
3. Solve equation (2.35) to obtain the generalized flow index for pipe flow
4. Determine the apparent viscosity for the drill pipe by applying $\tau_{w,p}$ and $\gamma_{w,p}$ to equation (2.47)
5. Calculate the generalized Reynolds number in equation (2.48) with the apparent viscosity from step 4.
6. Apply the generalized Reynolds number and determine the friction factor from equation (2.50) or (2.51) depending on the flow regime - use the generalized effective diameter from equation (2.43)
7. Employ the friction factor from step 6 to calculate the pressure loss from equation (2.52)

Annular flow

1. Give the flow rate and solve equation (2.30) to obtain the wall shear stress $\tau_{w,a}$
2. Use $\tau_{w,a}$ in equation (2.15) and solve for the wall shear rate $\gamma_{w,a}$
3. Solve equation (2.42) with the hydraulic diameter given in equation (2.25) to obtain the generalized flow index for annular flow
4. Determine the apparent viscosity for the annulus by applying $\tau_{w,a}$ and $\gamma_{w,a}$ to equation (2.47)
5. Calculate the generalized Reynolds number in equation (2.49) with the apparent viscosity from step 4.
6. Apply the generalized Reynolds number and determine the friction factor from equation (2.50) or (2.51) depending on the flow regime - use the generalized effective diameter from equation (2.44)
7. Employ the friction factor from step 6 to calculate the pressure loss from equation (2.53)

Nomenclature

D: pipe diameter, m
D_{eff}: effective diameter, m
D_h: hydraulic diameter, m
f: friction factor
K: consistency index, Pas^n
L: length, m

n: flow index

n': generalized flow index

P: pressure, Pa

Q: flow rate, m³/s

r: distance from annulus center, m

R: pipe radius, m

R_i: radius of inner cylinder, m

R_0: radius of outer cylinder, m

R_δ: annular clearance, m

Re_g: generalized Reynolds number

u: velocity, m/s

v: average velocity, m/s

γ: shear rate, s⁻¹

ε: pipe roughness

$\mu_{w,app}$: apparent viscosity at the wall, Pas

τ: shear stress, Pa

τ_0: yield stress, Pa

ρ: flud density, kg/ m³

Subscripts

a: annulus

N: Newtonian

p: pipe

w: wall

2.3.2 Bit pressure loss

Pressure loss over the bit nozzles may be derived by applying a continuity equation and Bernoulli's principle. The continuity equation gives:

$$Q = v_a A_a = v_b A_b = constant \tag{2.54}$$

where v is the velocity and A is the area at two arbitrary reference points a and b. Neglecting the gravitational term and assuming a frictionless and incompressible system, Bernoulli's principle for the pressure loss over the bit gives:

$$\frac{v_a{}^2}{2} + \frac{P_a}{\rho} = \frac{v_b{}^2}{2} + \frac{P_b}{\rho} \tag{2.55}$$

Reference points a and b in equation (2.55) corresponds to the drill pipe and bit nozzles respectively. By comparing drill pipe velocity with nozzle velocity, the drill pipe velocity is found negligible and equation (2.55) simplifies to:

$$\Delta P_{bit} = P_a - P_b = \frac{\rho}{2} v_b{}^2 \tag{2.56}$$

Experiments have shown that pressure loss across the bit is slightly different than predicted by the latter equation (Aadnøy, 2010). Therefore, a nozzle discharge coefficient is often introduced to improve the results. Applying the discharge coefficient and the continuity equation gives the pressure loss over the bit as

$$\Delta P_{bit} = \frac{\rho Q^2}{2A^2 K_d{}^2} \tag{2.57}$$

The discharge coefficient is normally set to 0.95 (Moore, 1974; Warren, 1989; Aadnøy, 2010). However, Warren (1989) conducted experiments on a large-scale drilling test machine to measure the pressure loss through roller cone bits and reported that using a discharge coefficient of 0.95 produce an average error of 14.7% compared to measurements. Results indicate that the pressure loss is in fact over predicted by equation (2.57) using the given value for the discharge coefficient. Other researchers have reported the same over prediction (Warren, 1989). A phenomenon referred to as pressure recovery is believed to have an impact on the discrepancies between calculated and measured values. The pressure recovery occurs when a fluid moves from a high velocity region in proximity of the bit nozzles to a lower velocity region in the annulus further away from the bit. When the velocity decreases, the pressure will increase according to Bernoulli's principle, and some of the pressure is thus recovered.

Still, Warren (1989) was unable to determine the actual effect the pressure recovery imposed on the discrepancy. Other flow effects were also discussed, and the pressure loss across the bit is believed to be of a more complex nature than proposed by equation (2.57). Examples of such effects are jet velocity, borehole pressure, nozzle- to bore-diameter ratio, and mud density. Despite the challenges of giving a definite explanation to the discrepancy, Warren (1989) provided an improvement of the nozzle discharge coefficient. Through experiments with different muds and after evaluating 770 data points, a value of 1.023 for roller cone bits gave an absolute mean error of 4.1%. Therefore, the proposed value of 1.023 is applied to equation (2.57) in this thesis. Note that this value only applies to roller cone bits. The discharge coefficient for different PDC bits did not follow a clear trend such as for roller cone bits.

Nomenclature

A: total nozzle area, m^2

K_d: nozzle discharge coefficient

P_a: drill pipe pressure, Pa

P_b: pressure at the bit nozzles, Pa

Q: flow rate, m^3/s

ΔP_{bit}: bit pressure loss, Pa

v: velocity, m/s

ρ: fluid density, kg/m^3

2.4 Energy source terms

There are many mathematical models that describe the temperature distribution of circulating drilling fluids. Raymond (1969) presented numerical solutions of the temperature profile for a circulating fluid system during transient and pseudo steady-state conditions. One year later, Holmes and Swift (1970) published an article that gives an analytical solution of the temperature distribution assuming steady-state heat transfer between the annulus and the drill pipe. Another study on the temperature of drilling fluids during circulation was given by Kabir et al. (1996). The intention of these models is to provide estimates of the temperature and a better understanding of downhole conditions that might occur during drilling operations. This information may be used to for example optimized mud selection. However, these models do not consider processes during a drilling operation that introduce additional heat to the wellbore system. Heat generation from energy sources present during drilling may have significant effect on the temperature distribution (Keller et al., 1973). To provide a more realistic solution, the following energy source terms are implemented in this work

1. Drill pipe rotation
2. Drill bit friction
3. Frictional pressure losses
4. Joule-Thomson coefficient

2.4.1 Drill pipe rotation

Friction refers to the force that resists relative motion of two solid objects in contact. The mechanical energy that exists in the process where two solid objects slide against each other is converted to heat. Researchers believe that practically all the dissipated energy related to frictional processes will be converted to heat (Bhushan, 2000).The energy dissipation which is termed frictional heating, results in a temperature increase at the interface between the two objects. In a deviated wellbore, the drill pipe tends to lay at the low side of the wellbore. Consequently, friction occurs at the drill pipe and casing/formation interface and heat is generated during rotation. The frictional force is proportional to the normal force applied by the drill pipe. In highly deviated sections or sharp bends and doglegs where the normal force may be large, a significant amount of heat can be generated. To quantify the amount of heat that is generated because of wellbore friction, the following equation is applied (Kumar & Samuel, 2013):

$$P_{wf} = \tau(\alpha) \cdot 2\pi \cdot rps \tag{2.58}$$

where P_{wf} is regarded as the heat rate or downhole power loss, τ is the torque acting on the drill pipe due to wellbore friction and rps represents the drill pipe rotations per second.

The torque is calculated by a 3D wellbore friction model given by Aadnoy, Fazaelizadeh, and Hareland (2010). This model gives an analytical solution of torque and drag that applies for straight sections, build-up-bends, drop-off-bends, side bends, and any combination of these situations. Additionally, it offers the opportunity to include the effect of combined axial motion and rotation. The equations that are applied to calculate the torque and thus the frictional heating due to wellbore friction is presented below. Note that combined motion is included here.

Straight sections

For a straight section, the torque that is acting on the drill pipe is expressed as

$$\tau = \mu r \beta w \Delta L \sin \alpha \cos \psi \tag{2.59}$$

Curved sections

For any type of bend, the axial force in the drill pipe is determined by

$$F_2 = F_1 + F_1 \left(e^{\pm |\theta_2 - \theta_1|} - 1 \right) \sin \psi + \beta w \Delta L \left[\frac{\sin \alpha_2 - \sin \alpha_1}{\alpha_2 - \alpha_1} \right] \tag{2.60}$$

where $+$ indicates tripping out and $-$ indicates tripping in. The parameters F_2 and F_1 refers to the axial force at the top and bottom of a drill pipe element of the length ΔL. Since this is a 3D model, the absolute change of direction is considered by implementing the dogleg. The dogleg may be determined from the equation below.

$$\cos \theta = \sin \alpha_1 \sin \alpha_2 \cos(\phi_1 - \phi_2) + \cos \alpha_1 \cos \alpha_2 \tag{2.61}$$

Here, the subscripts 1 and 2 represents two successive survey measurements. Finally, the torque for a curved section is determined by equation (2.62).

$$\tau = \mu r F_1 |\theta_2 - \theta_1| \cos \psi \qquad (2.62)$$

For all the equations above, ψ represents the angle between the axial and tangential pipe velocities during combined motion. The parameter is obtained from the following relationship:

$$\psi = \tan^{-1}\left(\frac{V_h}{V_r}\right) = \tan^{-1}\left(\frac{60V_h}{2\pi N_r r}\right) \qquad (2.63)$$

More details regarding the derivation of the model and corresponding theory is found in Aadnoy et al. (2010).

Nomenclature

F: axial force, N
L: length, m
N_r: rotary pipe speed, 1/min
P_{wf}: heat rate, J/s
r: pipe radius, m
rps: rotations per second, 1/s
V_h: axial pipe velocity, m/s
V_r: tangential pipe speed, m/s
w: unit pipe weight, N/m
α: angle of inclination, radians
β: buoyancy factor
θ: dogleg angle, radians
μ: friction factor
τ: torque, Nm
ϕ: azimuth, rad
ψ: angle between axial and tangential pipe velocities, radians

2.4.2 Drill bit friction

When the drill bit works on the formation to crush the rock, friction occurs at the interface of the bit and the formation and heat is generated. As stated previously, it is reasonable to assume that all the energy dissipation in this process is converted to thermal energy. However, it was also mentioned in chapter 2.1 that there seems to be a lack of research on how to quantify the amount of mechanical energy that is necessary to crush the rock and thus how large the potential of heat generation is. Keller et al. (1973) suggested that 40% of the mechanical input used to rotate the drill pipe is spent on drilling the formation. Corre et al. (1984) stated that depending on the lithology, about 10% of the mechanical input would be enough. Still, none of them gave any reasoning behind the proposed percentages, making it hard to assess who is more correct.

The intention of this thesis will therefore shift from quantifying the exact amount of heat generated from crushing the rock to evaluating the actual effect heat generation from the bit impose on the temperature distribution.

If the effect of frictional heating from the bit reveals to have a significant impact on the temperature distribution, it will be an advantage to have an idea of which parameters to adjust to control the heat generation. Mechanical specific energy (MSE) is a term that is commonly utilized as a measure of drilling efficiency. The term gives the energy required to remove a unit volume of rock (Hamrick, 2011). MSE is defined by the general expression:

$$MSE = \frac{total\ energy\ input}{volume\ removed} \tag{2.64}$$

The expression can also be given as (Hamrick, 2011)

$$MSE = \frac{WOB}{Area} + \frac{2\pi \cdot rpm \cdot \tau}{Area \cdot ROP} \tag{2.65}$$

The idea behind defining MSE is to use it as a tool for increasing drilling efficiency. Manipulating the operational parameters in equation (2.65) to minimize the MSE gives a favorable ratio of energy input to volume of rock removed. Keeping track of and minimizing MSE during an operation may also be used to minimize the heat generation from both the rotation of the pipe and the drilling of the formation as it is affected by the mechanical energy input.

Nomenclature

$Area$: wellbore area, m^2
ROP: rate of penetration, m/min
rpm: rotations per minute, 1/min
WOB: weight on bit, N
τ: torque, Nm

2.4.3 Frictional pressure losses

Another source of heat occurs as drilling fluid is circulated through the drill pipe and the annulus. Whenever a fluid flows through a pipe, a velocity gradient is present in the fluid. The velocity gradient appears because the fluid in contact with the pipe surface has zero velocity

according to the no-slip condition (Munson, Young, & Okiishi, 2006). Close to the wall, the velocity gradient will be large and layers of fluid will move relative to each other. The friction that occurs between these layers because of fluid viscosity, results in a pressure drop and consequently heat generation during circulation. In this thesis, all the mechanical energy required to overcome the pressure drop is converted to heat. The applied pressure loss calculations are given in chapter 2.3.

2.4.4 Joule-Thomson coefficient

As a liquid or a gas is either compressed or expanded, a subsequent change of temperature is experienced. Whether the temperature decreases or increases depends on the original state of the fluid. To consider this effect in the temperature model, the Joule-Thomson coefficient is implemented. The Joule-Thomson coefficient describes how the temperature of a fluid is affected by changes in pressure at constant enthalpy (Maghari & Safaei, 2007). The change of temperature due to pressure changes is mathematically described in the temperature model as

$$\mu_{JT} \frac{\Delta P}{\Delta x} \tag{2.66}$$

where μ_{JT} represents the Joule-Thomson coefficient. The approach from Alves, Alhanati, and Shoham (1992) has been employed to calculate the Joule-Thomson coefficient for the drilling fluid.

$$\mu_{JT} = \frac{1}{c_p} \left\{ T \left[\frac{\partial}{\partial T} \left(\frac{1}{\rho} \right) \right]_P - \frac{1}{\rho} \right\} \tag{2.67}$$

By introducing the linearized density model given in chapter 2.2.2, equation (2.67) becomes

$$\mu_{JT} = \frac{1}{c_p} \left\{ T \frac{\rho_0 \alpha}{\left(\rho_0 + \frac{\rho_0}{\beta}(P-P_0) - \rho_0 \alpha(T-T_0) \right)^2} - \frac{1}{\rho_0 + \frac{\rho_0}{\beta}(P-P_0) - \rho_0 \alpha(T-T_0)} \right\} \tag{2.68}$$

The Joule-Thomson coefficient may take a positive or negative sign. The point at which the sign changes is referred to as the inversion point (Maghari & Safaei, 2007). As an example, the sign for water will stay negative given that the temperature is below 250 °C. With the range of

temperature experienced in this thesis, the sign of the Joule-Thomson coefficient for the considered drilling fluid is also found to stay negative. A negative sign indicates that the drilling fluid will heat as it expands and cool as it compresses. Consequently, the reduction in pressure with the flow direction in the annulus will introduce heat to the system. However, a reduction of temperature occurs in the drill pipe as the pressure increases with the flow direction.

Nomenclature

c_p: specific heat capacity, J/kg°C
P: pressure, Pa
P_0: pressure at point of linearization, Pa
T: temperature, °C
T_0: temperature at point of linearization, °C
x: measured depth, m
α: cubical expansion coefficient, 1/°C
β: isothermal bulk modulus, Pa
μ_{JT}: Joule-Thomson coefficient, °C/Pa
ρ: drilling fluid density, kg/m^3

2.5 Temperature model

2.5.1 Derivation

A derivation of the developed temperature model is presented below, where figure 2-4 represents a general wellbore element at which the derivation is based on. In the drill pipe, the flow direction is set downwards and heat will therefore enter the system at x and leave the system at $x + dx$. Heat will also enter the system due to heat transfer with the annulus and heat generation from additional energy sources within the drill pipe. Consequently, the energy balance for the wellbore element is expressed by:

$$Q_{p(x+dx)} - Q_{p(x)} = Q_{ap} + \phi_p \tag{2.69}$$

where Q_{ap} represents the rate of heat transfer with the annulus and ϕ_p represents the energy sources present within the drill pipe. The change in thermal energy over the element is given by (Bergman et al., 2011):

$$Q_{p(x+dx)} - Q_{p(x)} = mc_{pp}\left(T_{p(x+dx)} - T_{p(x)}\right) \tag{2.70}$$

while the heat transfer across the drill pipe is expressed as (Kabir et al., 1996)

$$Q_{ap} = 2\pi r_{pi} U_p \left(T_a - T_p\right) dx \tag{2.71}$$

where r_{pi} is the inner radius of the drill pipe and U_p represents the overall heat transfer as explained in chapter 2.2.1. Combining equations (2.69-2.71) gives the following differential equation for the drill pipe temperature distribution:

$$\frac{dT_p}{dx} = AT_a - AT_p + \frac{1}{mc_{pp}} \frac{\phi_p}{dx} \tag{2.72}$$

where

$$A = \frac{2\pi r_{pi} U_p}{mc_{pp}} \tag{2.73}$$

For the annulus, the flow direction is set upwards and heat will consequently enter the system at $x + dx$ and leave the system at x. Additional heat enters the system by heat transfer from the

formation and heat generation due to energy sources in the annulus, and heat will also leave the system through the interface with the drill pipe. The energy balance for the wellbore element becomes:

$$Q_{a(x+dx)} - Q_{a(x)} = Q_{ap} - Q_f - \phi_a \tag{2.74}$$

where Q_f gives the heat transfer from the formation to the wellbore interface and ϕ_a represents the energy sources in the annulus. Following Bergman et al. (2011), the thermal energy over the annulus element may be expressed by:

$$Q_{a(x+dx)} - Q_{a(x)} = m c_{pa} \left(T_{a(x+dx)} - T_{a(x)} \right) \tag{2.75}$$

The rate of heat transfer across the drill pipe remains the same as in equation (2.71) and the heat flow from the formation to the wellbore is given in the equation below (Kabir et al., 1996).

$$Q_f = \frac{2\pi k_f}{T_D} \left(T_f - T_w \right) dx \tag{2.76}$$

Here, T_w is the temperature at the interface between the formation and the wellbore. An approximation for the dimensionless temperature T_D in equation (2.76), is determined by the equations given in chapter 2.1. The heat transfer from the wellbore/formation interface to the annulus is given in equation (2.77).

$$Q_{wa} = 2\pi r_{ci} U_a (T_w - T_a) dx \tag{2.77}$$

Combining equation (2.76) and (2.77) to eliminate T_w, the heat flow from the formation to the annulus is expressed by:

$$Q_f = \frac{2\pi r_{ci} U_a k_f}{k_f + r_{ci} U_a T_D} \left(T_f - T_a \right) dx \tag{2.78}$$

Updating the energy balance in equation (2.74) with the expressions in equations (2.71), (2.75) and (2.78) yields the differential equation for the annulus temperature distribution as shown below.

$$\frac{dT_a}{dx} = C(T_a - T_p) - B(T_f - T_a) - \frac{1}{mc_{pa}}\frac{\phi_a}{dx} \tag{2.79}$$

where

$$C = \frac{2\pi r_{pi}U_p}{mc_{pa}} \tag{2.80}$$

$$B = \frac{2\pi r_{ci}U_a k_f}{(k_f + r_{ci}U_a T_D)mc_{pa}} \tag{2.81}$$

Considering equations (2.72) and (2.79), there is a set of two equations and two unknowns, explicitly T_p and T_a .To take the derivation further, equation (2.72) is rearranged to the following form:

$$T_a = \frac{1}{A}\frac{dT_p}{dx} + T_p - \frac{1}{A}\frac{1}{mc_{pp}}\frac{\phi_p}{dx} \tag{2.82}$$

Substituting T_a in equation (2.79) with the expression above and solving for T_p gives

$$\frac{d^2 T_p}{dx^2} - D\frac{dT_p}{dx} - ABT_p = g(x) \tag{2.83}$$

where

$$D = -A + B + C \tag{2.84}$$

and

$$g(x) = -ABT_f - \frac{B+C}{mc_{pp}}\frac{\phi_p}{dx} - \frac{A}{mc_{pa}}\frac{\phi_a}{dx} \tag{2.85}$$

Before proceeding, it is important to acknowledge that the chosen derivation procedure contains a constraint. The differential equation in (2.83) is solved by utilizing the Undetermined Coefficients method. This method requires that the coefficients A, B, and C are constants. On the contrary, these coefficients are not constant throughout the wellbore because they involve the overall heat transfer coefficient. The overall heat transfer coefficient contains temperature dependent parameters such as drilling fluid density and viscosity and neither A, B, or C can be regarded as constants for the length of the wellbore. An analytical solution is consequently not achievable.

Numerical approach

Because of the constraint mentioned in the latter paragraph, a numerical approach is implemented to obtain a solution of the wellbore temperature distribution. Using a numerical approach allows the wellbore to be divided into a certain number of boxes. For each box, all the parameters that varies throughout the wellbore are updated and treated as constants over the box length, which allows equation (2.80) to be solved by the Undetermined Coefficients method. Since a numerical approach is implemented, the notation of the discretized wellbore given in figure 2-5 is now employed. Here, i refers to a random box in the discretized wellbore.

The formation temperature T_f in equation (2.85) varies with depth. For a vertical wellbore, it is common to express the formation temperature with a constant surface temperature and a linear geothermal gradient such as in equation (2.86).

$$T_f(x) = T_s + Gx \tag{2.86}$$

But the objective of this work is to develop a temperature model for deviated wellbores. Taking advantage of the numerical approach, the following function has been implemented:

$$T_{f(i)} = T_{f(i-1)} + G \cos\left(I_{(i)}\right)\left(x_{(i)} - x_{(i-1)}\right) \tag{2.87}$$

Here, $T_{f(i-1)}$ and $x_{(i-1)}$ refers to the formation temperature and the measured depth at box $i-1$, and $x_{(i)}$ and $I_{(i)}$ represents measured depth and the angle of inclination for box i. Equation (2.83) can now be expressed as

$$\frac{d^2 T_{p(i)}}{dx^2} - D\frac{dT_{p(i)}}{dx} - ABT_{p(i)} = -AB\left[T_{f(i-1)} + G\cos\left(I_{(i)}\right)\left(x_{(i)} - x_{(i-1)}\right)\right] \tag{2.88}$$
$$- \frac{B+C}{mc_{pp}}\frac{\phi_{p(i)}}{dx} - \frac{A}{mc_{pa}}\frac{\phi_{a(i)}}{dx}$$

Finally, solving the second order inhomogeneous differential equation above yields the general expression for the temperature distribution in the drill pipe:

$$T_{p(i)} = C_1 e^{\theta_1 x_{(i)}} + C_2 e^{\theta_2 x_{(i)}} + T_{f(i-1)} + G\cos\left(I_{(i)}\right)x_{(i)} - G\cos\left(I_{(i)}\right)x_{(i-1)} \tag{2.89}$$

$$-\frac{D}{AB}G\cos\left(I_{(i)}\right) + \frac{B+C}{AB}\frac{1}{mc_{pp}}\frac{\phi_{p(i)}}{dx} + \frac{1}{Bmc_{pa}}\frac{\phi_{a(i)}}{dx}$$

Furthermore, substituting equation (2.89) for T_p in equation (2.82) gives the general solution of the temperature distribution in the annulus.

$$T_{a(i)} = \left(1 + \frac{\theta_1}{A}\right)C_1 e^{\theta_1 x_{(i)}} + \left(1 + \frac{\theta_2}{A}\right)C_2 e^{\theta_2 x_{(i)}} + T_{f(i-1)} + G\cos\left(I_{(i)}\right)x_{(i)} - G\cos\left(I_{(i)}\right)x_{(i-1)}$$

$$+\left(\frac{1}{A} - \frac{D}{AB}\right)G\cos\left(I_{(i)}\right) + \left(\frac{B+C}{AB} - \frac{1}{A}\right)\frac{1}{mc_{pp}}\frac{\phi_{p(i)}}{dx} + \frac{1}{Bmc_{pa}}\frac{\phi_{a(i)}}{dx} \tag{2.90}$$

where

$$\theta_1 = \frac{D + \sqrt{D^2 + 4AB}}{2} \tag{2.91}$$

$$\theta_2 = \frac{D - \sqrt{D^2 + 4AB}}{2} \tag{2.92}$$

Equations (2.89) and (2.90) are solved to determine the wellbore temperature distribution for each box in the wellbore. Note that the following coefficients that are not constant, must be determined for each box:

$$C_1, C_2, \theta_1, \theta_2, A, B, C, D$$

Also, note that equations (2.87), (2.89), and (2.90) are valid for:

$$x_{(i-1)} \leq x \leq x_{(i)}$$

Energy source terms

A summary of the source terms that are included in the different regions of the wellbore is given in table 2-3.
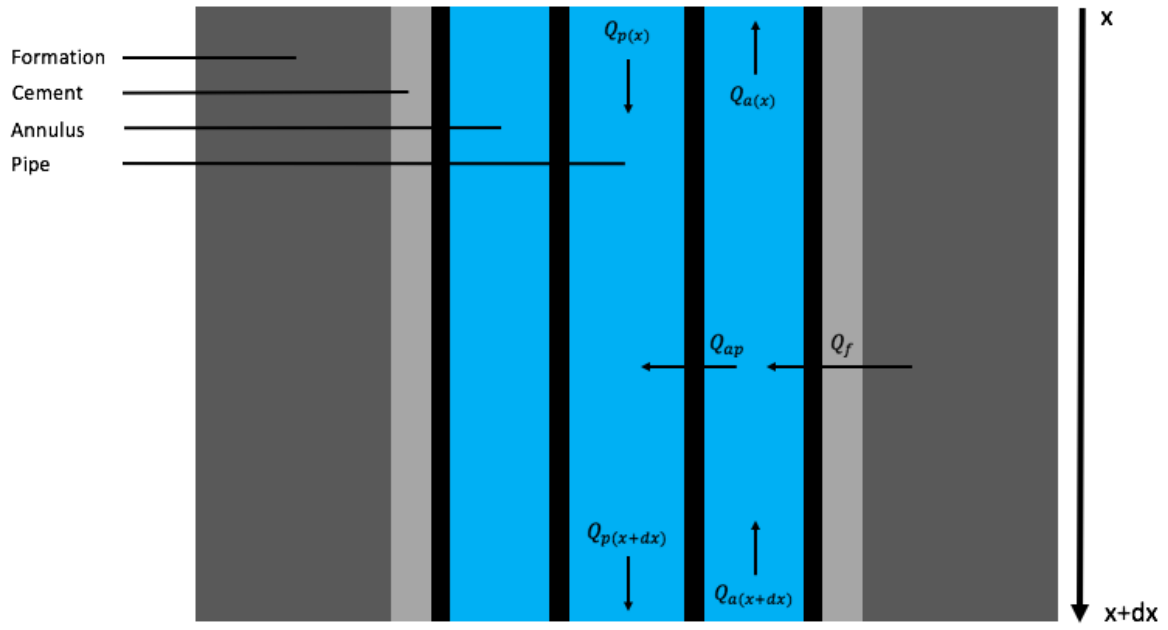
Figure 2-4 Wellbore element
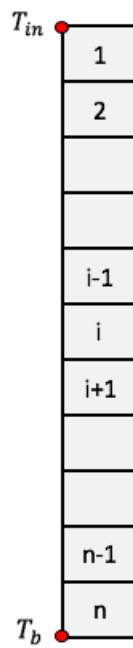
Figure 2-5 Discretized wellbore

Drill pipe	Bottom of the wellbore	Annulus
-	drill pipe rotation	drill pipe rotation
-	drill bit friction	-
frictional pressure losses	frictional pressure losses	frictional pressure losses
Joule-Thomson coefficient	Joule-Thomson coefficient	Joule-Thomson coefficient

Table 2-3 Energy source terms

Nomenclature

c_p: specific heat capacity, J/kg°C
G: geothermal gradient, °C/m
k: thermal conductivity, W/m°C
m: mass rate, kg/s
Q: rate of heat, J/s
r: radius, m
T: temperature, °C
T_D: dimensionless temperature
U: overall heat transfer coefficient, W/m²°C
x: measured depth, m
ϕ: energy source term, J/s

Subscripts

p: drill pipe
a: annulus
f: formation
w: wellbore
i: inner
c: casing
s: surface

2.5.2 Algorithm

This chapter presents the algorithm applied to obtain a solution for the wellbore temperature distribution. The procedure starts at the bottom of the well and relies on a given temperature to calculate the temperature distribution throughout the wellbore. Consider the illustration in figure 2-5. Here, the wellbore is divided into a certain number of boxes. The bottom of the wellbore and the total number of boxes, is represented by the letter n. At this point, it is necessary to give an initial guess of the bottom hole temperature as a boundary condition. A reasonable choice of boundary condition for a drilling operation is:

$$T_{p(n)} = T_{a(n)} = T_b$$

where T_b represents the guess of wellbore temperature at the bottom of box number n, as indicated by the red mark in figure 2-5. The corresponding depth and angle of inclination are given by:

$$x = dx * n$$

$$I = I_{(n)}$$

where x is the measured depth and dx is the measured depth of a single box.

Substituting T_p and T_a with T_b in equations (2.89) and (2.90) gives a system of equations with two variables, explicitly $C_{1(n)}$ and $C_{2(n)}$.

$$T_b = C_{1(n)}e^{\theta_1 dx*n} + C_{2(n)}e^{\theta_2 dx*n} + T_{f(n-1)} + G\cos(I_{(n)})dx - \frac{D}{AB}G\cos(I_{(n)}) + \frac{B+C}{AB}\frac{1}{mc_{pp}}\frac{\phi_{p(n)}}{dx}$$

$$+ \frac{1}{Bmc_{pa}}\frac{\phi_{a(n)}}{dx} \tag{2.93}$$

$$T_b = \left(1 + \frac{\theta_1}{A}\right)C_{1(n)}e^{\theta_1 dx*n} + \left(1 + \frac{\theta_2}{A}\right)C_{2(n)}e^{\theta_2 dx*n} + T_{f(n-1)} + G\cos(I_{(n)})dx$$

$$+ \left(\frac{1}{A} - \frac{D}{AB}\right)G\cos(I_{(n)}) + \left(\frac{B+C}{AB} - \frac{1}{A}\right)\frac{1}{mc_{pp}}\frac{\phi_{p(n)}}{dx} + \frac{1}{Bmc_{pa}}\frac{\phi_{a(n)}}{dx} \tag{2.94}$$

Here, equations (2.89) and (2.90) have also been updated with the following relation:

$$G\cos(I_{(n)})dx * n - G\cos(I_{(n)})dx * (n-1) = G\cos(I_{(n)})dx$$

In this case, equations (2.93) and (2.94) are valid for:

$$dx * (n-1) \leq x \leq dx * n$$

A convenient method to solve equations (2.93) and (2.94) for $C_{1(n)}$ and $C_{2(n)}$ is matrix multiplication. The coefficients $C_{1(n)}$ and $C_{2(n)}$ can be determined by rearranging equations (2.93) and (2.94) to the following form:

$$\begin{bmatrix} C_{1(n)} \\ C_{2(n)} \end{bmatrix} = \begin{bmatrix} a & b \\ c & d \end{bmatrix}^{-1} \begin{bmatrix} y_1 \\ y_2 \end{bmatrix}$$

where

$$a = e^{\theta_1 dx * n}$$

$$b = e^{\theta_2 dx * n}$$

$$c = \left(1 + \frac{\theta_1}{A}\right) e^{\theta_1 dx * n}$$

$$d = \left(1 + \frac{\theta_2}{A}\right) e^{\theta_2 dx * n}$$

$$y_1 = T_b - \left(T_{f(n-1)} + G\cos(I_{(n)})\,dx - \frac{D}{AB} G\cos(I_{(n)}) + \frac{B+C}{AB}\frac{1}{mc_{pp}}\frac{\phi_{p(n)}}{dx} + \frac{1}{Bmc_{pa}}\frac{\phi_{a(n)}}{dx}\right)$$

$$y_2 = T_b - \left(T_{f(n-1)} + G\cos(I_{(n)})\,dx + \left(\frac{1}{A} - \frac{D}{AB}\right) G\cos(I_{(n)}) + \left(\frac{B+C}{AB} - \frac{1}{A}\right)\frac{1}{mc_{pp}}\frac{\phi_{p(n)}}{dx} + \frac{1}{Bmc_{pa}}\frac{\phi_{a(n)}}{dx}\right)$$

Assuming the coefficients $C_{1(n)}$ and $C_{2(n)}$ are constant for box n, $T_{p(n-1)}$ and $T_{a(n-1)}$ are calculated at the boundary between box n and box $n-1$ by using $C_{1(n)}$ and $C_{2(n)}$ in equations (2.86) and (2.87) respectively. Note that the depth and angle of inclination at this point are given by:

$$x = dx(n-1)$$

$$I = I_{(n)}$$

After $T_{p(n-1)}$ and $T_{a(n-1)}$ have been determined, they will serve as the boundary temperatures for box number $n-1$, and $C_{1(n-1)}$ and $C_{2(n-1)}$ are calculated with the same approach as above to obtain $T_{p(n-2)}$ and $T_{a(n-2)}$. This procedure is repeated for the remaining boxes to get the

total wellbore temperature distribution. In a general notation, $C_{1(i)}$ and $C_{2(i)}$ are calculated based on the boundary temperatures $T_{p(i)}$ and $T_{a(i)}$ and used in equations (2.89) and (2.90) to obtain $T_{p(i-1)}$ and $T_{a(i-1)}$. The depth and angle of inclination for box number i becomes:

$$x = dx(i-1)$$

$$I = I_{(i)}$$

When $i = 1$ and box number 1 is reached, the depth and the angle of inclination will be

$$x = 0$$

$$I = I_{(1)}$$

and equations (2.89) and (2.90) reduce to

$$T_{p(0)} = C_{1(1)} + C_{2(1)} + T_{f(0)} - \frac{D}{AB} G \cos(I_{(1)}) + \frac{B+C}{AB} \frac{1}{mc_{pp}} \frac{\phi_{p(1)}}{dx} + \frac{1}{Bmc_{pa}} \frac{\phi_{a(1)}}{dx} \quad (2.95)$$

$$T_{a(0)} = \left(1 + \frac{\theta_1}{A}\right) C_{1(1)} + \left(1 + \frac{\theta_2}{A}\right) C_{2(1)} + T_{f(0)} + \left(\frac{1}{A} - \frac{D}{AB}\right) G \cos(I_{(1)}) + \left(\frac{B+C}{AB} - \frac{1}{A}\right) \frac{1}{mc_{pp}} \frac{\phi_{p(1)}}{dx}$$

$$+ \frac{1}{Bmc_{pa}} \frac{\phi_{a(1)}}{dx} \quad (2.96)$$

With this last step, the temperature distribution for the entire wellbore has been calculated. To summarize, consider the following stepwise approach as a representation of the algorithm for calculating the wellbore temperature distribution:

1. Give a guess for the bottom hole temperature T_b
2. Determine the coefficients $C_{1(n)}$ and $C_{2(n)}$
3. Calculate $T_{p(n-1)}$ and $T_{a(n-1)}$
4. Set $i = n - 1$ and update the coefficients that are not constant
5. Determine $C_{1(i)}$ and $C_{2(i)}$
6. Calculate $T_{p(i-1)}$ and $T_{a(i-1)}$

7. Set $i = i - 1$ and repeat step 4 to 6

8. Stop when $i = 1$

Nomenclature

c_p: specific heat capacity, J/kg°C
dx: box length, m
G: geothermal gradient, °C/m
I: angle of inclination, deg
m: mass rate, kg/s
n: number of boxes
T: temperature, °C
x: measured depth, m
ϕ: energy source term, J/s

Subscripts

a: annulus
b: bottom
f: formation
i: arbitrary box number
in: inlet
n: total number of boxes
p: pipe

2.5.3 Shooting method

The algorithm in chapter 2.5.2 may be defined as a boundary value problem with the following set of equations and boundary conditions:

$$T_{p(i)} = C_1 e^{\theta_1 x_{(i)}} + C_2 e^{\theta_2 x_{(i)}} + T_{f(i-1)} + G \cos(I_{(i)}) x_{(i)} - G \cos(I_{(i)}) x_{(i-1)} - \frac{D}{AB} G \cos(I_{(i)})$$

$$+ \frac{B+C}{AB} \frac{1}{mc_{pp}} \frac{\phi_{p(i)}}{dx} + \frac{1}{Bmc_{pa}} \frac{\phi_{a(i)}}{dx}$$

$$T_{a(i)} = \left(1 + \frac{\theta_1}{A}\right) C_1 e^{\theta_1 x_{(i)}} + \left(1 + \frac{\theta_2}{A}\right) C_2 e^{\theta_2 x_{(i)}} + T_{f(i-1)} + G \cos(I_{(i)}) x_{(i)} - G \cos(I_{(i)}) x_{(i-1)}$$

$$+ \left(\frac{1}{A} - \frac{D}{AB}\right) G \cos(I_{(i)}) + \left(\frac{B+C}{AB} - \frac{1}{A}\right) \frac{1}{mc_{pp}} \frac{\phi_{p(i)}}{dx} + \frac{1}{Bmc_{pa}} \frac{\phi_{a(i)}}{dx}$$

$$T_{p(n)} = T_{a(n)} = T_b$$

$$T_{p(0)} = T_{in}$$

where T_{in} is the drill pipe inlet temperature. The problem is solved by utilizing the shooting method, which is a numerical solution of boundary value problems. In general, the idea of this method is to reduce boundary value problems to initial value problems. This is achieved by considering one of the boundary conditions to be a known initial value and solving the problem with the objective of finding the initial value that satisfies the other boundary condition.

Take figure 2-6 as a representation of the boundary value problem presented above. The left boundary illustrates box number n and the bottom of the wellbore. Following the shooting method, a guess is made for T_b to calculate the total wellbore temperature distribution, thus redefining T_b from a boundary condition to a known initial value and reducing the problem to an initial value problem. If the guess of T_b results in a temperature distribution where $T_p(0)$ satisfies the boundary condition at $x = 0$, the problem is solved. If the boundary condition is not satisfied, T_b is adjusted until the solution converges.

The structure of the calculation procedure used to implement the shooting method is shown in figure 2-7. In the main program, the initial guess of T_b is defined. After defining the input value, the main program calls for "itsolver_t" to provide the solution of the initial value problem. The function "itsolver_t" is based on a nonlinear algebraic equation solver called the Bisection Method. The Bisection Method is a root finder that solves problems on the form

$$f(x) = 0$$

This approach takes advantage of the Intermediate Value Theorem which states that if $f(x)$ is a continuous function for a given interval $[a, b]$ and $f(a)$ and $f(b)$ have opposite signs, there must be a point c on the interval $[a, b]$ that gives $f(c) = 0$. An illustration of this statement is presented in figure 2-8. The Bisection Method finds the root of $f(x)$ by repeatedly bisecting the interval $[a, b]$ until a there is a midpoint c in the interval such that $f(c)$ converges to 0. Normally, a tolerance is set such that a solution is accepted when

$$abs[f(c)] < tolerance$$

To apply the Bisection Method to the current calculation procedure, the initial interval $[a, b]$ is defined based on T_b and f is defined as

$$(T_b) = T_p(0) - T_{in} = g(T_b) - T_{in}$$

For each iteration, the function "itsolver_t" calls for "temperature_bt" with the inputs given in table 2-4 to provide f. The function "temperature_bt" contains the algorithm explained in chapter 2.5.2. A while loop runs in "itsolver_t" until the following condition is met:

$$abs[T_p(0) - T_{in}] < tolerance$$

Finally, the shooting method has provided a value of T_b that satisfies the boundary value problem stated in the beginning of this chapter.
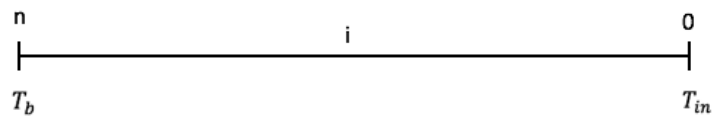
Figure 2-6 Boundary problem
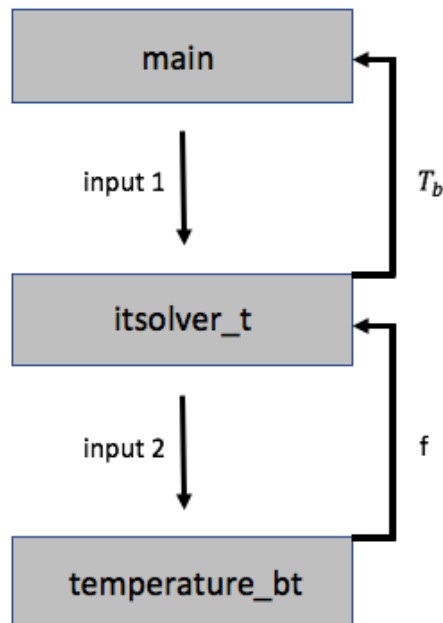
Figure 2-7 Flowchart of the Shooting Method
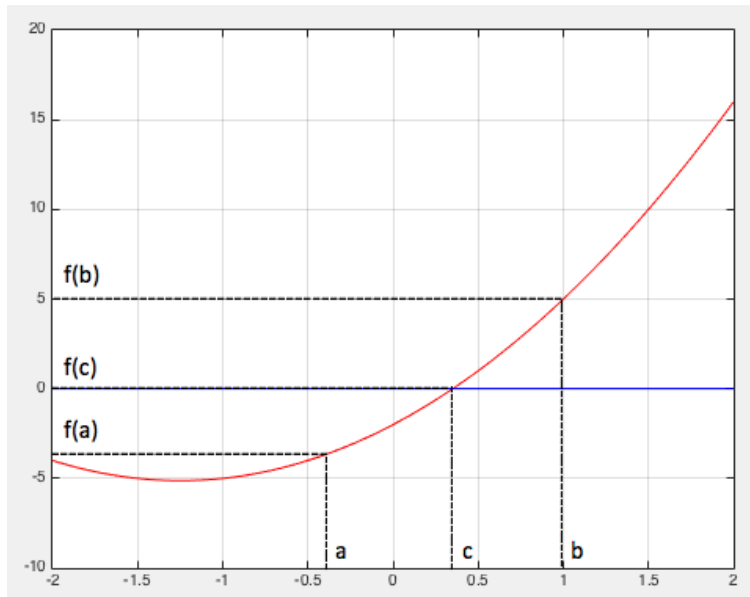
Figure 2-8 Intermediate Value Theorem

Parameter	Input 1	Input 2
T_b	✓	-
a	-	✓
b	-	✓
c	-	✓

Table 2-4 Input parameters

Nomenclature

a: start of interval, °C
b: end of interval, °C
c: midpoint of interval, °C
E: energy, J/s
I: angle of inclination, deg.
n: number of boxes
P: pressure, Pa
T: temperature, °C

x: measured depth, m
μ: viscosity, Pas

Subscripts

a: annulus
f: formation
in: inlet
p: pipe
R: rotation
s: surface

3 Results and discussion

3.1 Introduction

In this section, a sensitivity analysis of the developed temperature model is presented with respect to a drilling operation. The objective is to determine to what extent a set of parameters of the temperature model will impact the temperature distribution. Results are compared to a base case to determine the effect of each parameter. For the analysis of a given parameter, all the other parameters of the base case remain constant while investigating a range for the given parameter unless specified otherwise. The set of parameters for the base case is given in table 3-1. The sensitivity analysis is based on a scenario where an 8.5-inch section is drilled using a 5-inch drill pipe. Figure 3-1 illustrates the wellbore trajectory for the base case, which starts with a vertical section before kicking off to a deviated section with a constant inclination of 45 degrees from vertical. The total length of the wellbore is 2500 meters MD and there is no change in azimuth. At the top of the trajectory, the drill pipe inlet temperature and the initial formation temperature are defined. Note that the top of the trajectory is not supposed to represent the surface, but rather a start depth of choice. Therefore, the initial formation temperature for the base cases is set to 30 ℃. As an example, taking a subsea well with 4 ℃ at the seabed and a geothermal gradient of 30 ℃ per kilometer will give a formation temperature of 30 ℃ at approximately 850 meters below the seabed.
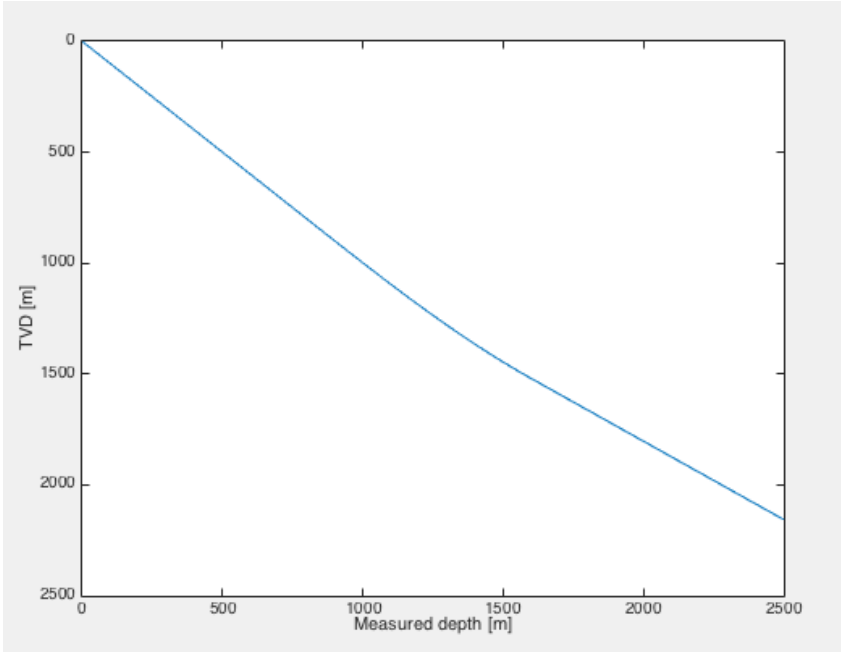
Figure 3-1 Wellbore trajectory

c_p	4182	J/kg°C
G	0.03	°C/m
I	45	degrees
k	0.6	W/m°C
k_f	2.25	W/m°C
k_p	50	W/m°C
q	1500	l/min
T_{fi}	30	°C
T_{in}	20	°C
ρ	1205	kg/m3

Table 3-1 Base case parameters

Nomenclature

$c_\square$: drilling fluid specific heat capacity, J/kg°C
G: geothermal gradient, °C/m
I: wellbore inclination, degrees
k: drilling fluid thermal conductivity, W/m°C
q: flow rate, l/min
T_{fi}: initial formation temperature, °C
T_{in}: drill pipe inlet temperature, °C
ρ: drilling fluid density, kg/m^3

Subscripts

f: formation
p: drill pipe

3.2 Base case

For the base case, the energy source terms discussed in chapter 2.4 are neglected, which basically means that this is a circulation scenario. The resulting wellbore temperature distribution is shown in figure 3-2, where the blue and red curves illustrate the drilling fluid temperature distribution in the drill pipe and the annulus. The formation temperature indicated by the black curve, is calculated based on the non-linear geothermal gradient given in equation (2.87).

The temperature of the fluid at the drill pipe inlet is 20 °C. This satisfies the boundary value problem discussed in chapter 2.5.3, where the condition of $T_{p(0)} = T_{in}$ was set. Moving down the drill pipe, the temperature increases due to heat flow from the relatively warmer annulus

fluid. At the bottom of the wellbore, the temperatures in the drill pipe and the annulus are equal, indicating that the other boundary condition of $T_{p(n)} = T_{a(n)}$ is satisfied. Another observation is that the maximum temperature in the wellbore occurs further up in the annulus and not at the bottom, which is a consequence of the boundary condition. The temperature distribution in the annulus is a result of heat transfer with both the formation and the drill pipe. Consider the depth of 1000 meters in figure 3-2. Here, the annulus fluid will gain heat from the formation and give heat to the drill pipe. Close to the top of the wellbore on the other hand, the temperature in the annulus exceeds both the formation and the drill pipe temperature, resulting in a heat loss from the annulus to both interfaces.
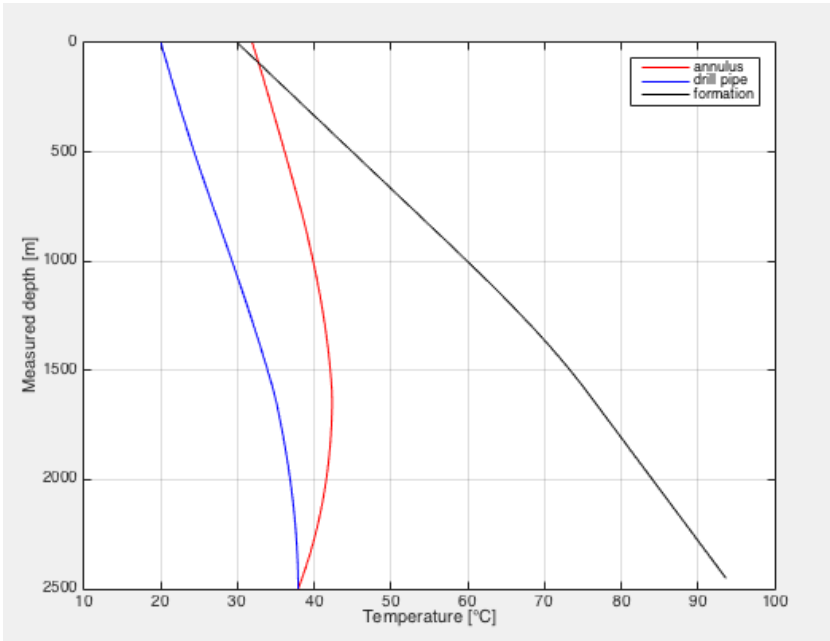
Figure 3-2 Temperature distribution - base case results

3.3 Flow rate

Flow rate is a critical parameter for the temperature distribution. It is a factor in several of the heat transfer processes that are included in the temperature model. Additionally, frictional pressure losses are approximately proportional to the square of the flow velocity. Changes in flow rate will therefore affect the wellbore pressure distribution and thus the pressure dependent properties such as drilling fluid density and viscosity. To investigate the effect of flow rate on the temperature distribution, simulations have been performed using the base case with varying

flow rates from 100 l/min to 2250 l/min. The results of flow rates at 500 l/min and 2000 l/min are given by figures 3-3 and 3-4 respectively.

Inspecting the results reveal that the flow rate imposes a significant effect. The bottom hole temperature for a flow rate of 500 l/min has increased with more than 30% compared to the base case results given in figure 3-2. On the contrary, increasing the flow rate results in a decrease of bottom hole temperature as illustrated by the results of 2000 l/min. The results also reveal that for a general reduction in flowrate, the entire temperature distribution will shift towards higher temperatures, and increasing the flow rate will shift the temperature distribution towards lower temperatures.

Another effect is that for increasing flow rates, the temperature distributions in the drill pipe and the annulus approach each other. For a flow rate of 500 l/min, the temperature difference between the drill pipe inlet and the annulus outlet is approximately 17 °C. The simulation results with a flow rate of 2000 l/min give a temperature difference of only 10 °C. Considering the equation below might explain the effect.

$$Q_{ap} = 2\pi r_{pi} U_p (T_a - T_p) dx$$

(2.71)

Equation (2.71) gives the rate of heat transfer between the annulus and the drill pipe. Here, the overall heat transfer U_p is determined by:

$$\frac{1}{U_p} = \frac{1}{h_p} + \frac{r_{pi}}{r_{po}} \frac{1}{h_a} + \frac{r_{pi}}{k_p} \ln\left(\frac{r_{po}}{r_{pi}}\right)$$

(2.6)

and the CHTC is calculated from equation (2.13) given that the flow is turbulent.

$$h = 0.023 \left(\frac{\rho v D}{\mu}\right)^{0.8} \left(\frac{c_p \mu}{k}\right)^n \frac{k}{D}$$

(2.13)

Consequently, increasing the flow rate will increase the CHTC, the overall heat transfer and thus the rate of heat transfer between the annulus and the drill pipe. This will lead to less thermal resistance between the annulus and the drill pipe and less difference in the temperature distributions.

The increase of flow rate will also result in a more even temperature distribution throughout the wellbore. Looking at the results for 500 l/min, there is a noticeable change of temperature in the annulus from the bottom of wellbore to the annulus outlet. As the flow rate increases, the change is less obvious and the temperature gradient in the annulus will reduce. For the case of 2000 l/min, the difference between the bottom hole temperature and the temperature at the annulus outlet is less than 5 °C. These results may be justified by looking at equation (2.75) and rearranging it to the following form:

$$\left(T_{a(x+dx)} - T_{a(x)}\right) = \frac{Q_{a(x+dx)} - Q_{a(x)}}{mc_{pa}}$$

Here, the flow rate is represented in the form of mass rate. Increasing the flow rate and thus the mass rate will decrease the temperature difference across a wellbore element and give a more even temperature distribution.

The simulation results for the entire range of flow rates from 100 l/min to 2250 l/min is given in figure 3-5. Figure 3-5 shows the variation in maximum, bottom hole, and annulus outlet temperature with flow rate. This plot indicates that the change in maximum and bottom hole temperature in the wellbore is significant for varying flow rates. The variation is less pronounced for the outlet temperature.
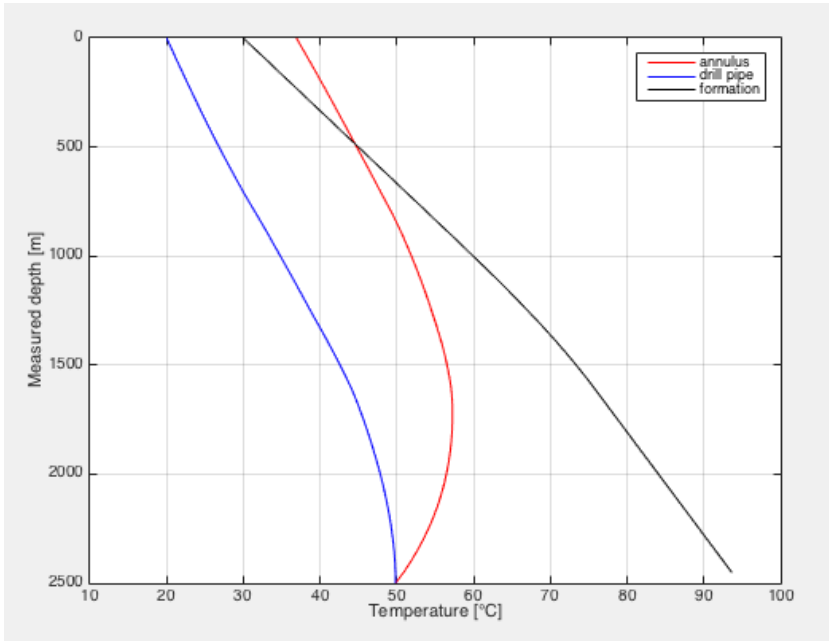
Figure 3-3 Temperature distribution - flow rate: 500 l/min
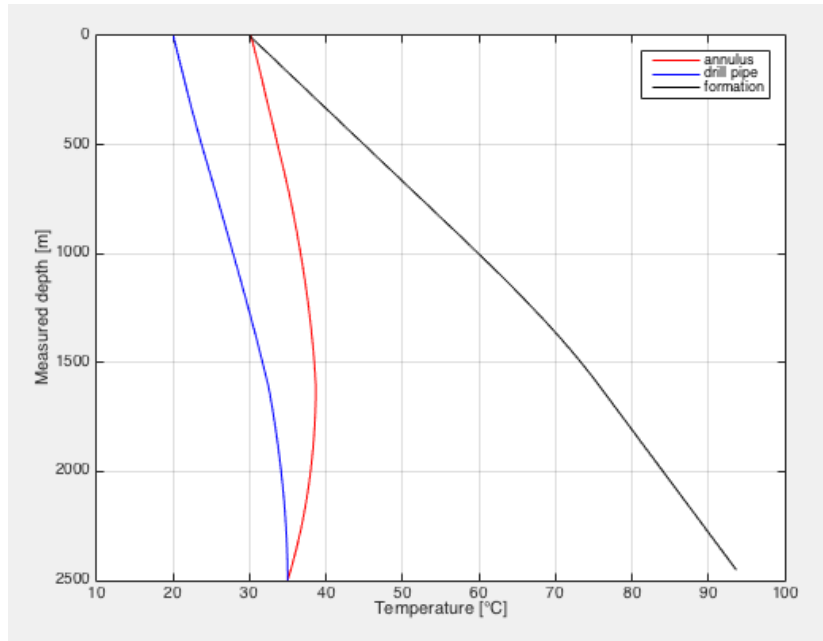
Figure 3-4 Temperature distribution - flow rate: 2000 l/min
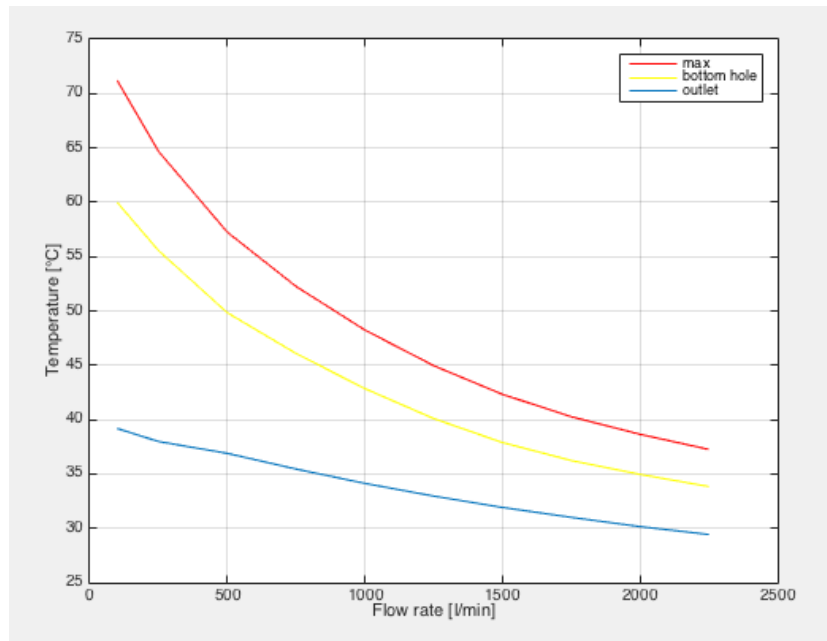
Figure 3-5 Temperature vs. flow rate

3.4 Specific heat capacity

Specific heat capacity is defined as the amount of heat per unit mass required to increase the temperature of an object by one Kelvin (Schroeder, 2000). A material with a low specific heat capacity will therefore need less energy to increase its temperature by a given amount compared to a material with a high specific heat capacity. Water has a high specific heat capacity. The value for pure liquid water is 4182 J/kg-°C at 20 °C, which is the value used in the base case. To determine how sensitive the wellbore temperature distribution is to drilling fluid specific heat capacity, simulations are performed with values in the range of 2000-4500 J/kg-°C.

Figures 3-6 and 3-7 show the results for specific heat capacities of 3000 and 2000 J/kg-°C respectively. Comparing these results to the base case, it is evident that decreasing the specific heat capacity will increase the temperatures in the wellbore. The maximum temperatures for the given cases have increased with 38% and 16% compared to the base case, indicating that the specific heat capacity has a significant effect on the temperature distribution. Another trend is that the annulus temperature distribution approaches the formation temperature and higher annulus temperature gradients are observed as the specific heat capacity is decreased. As discussed in the latter paragraph, an object with a low specific heat capacity will need less energy to increase its temperature by a certain amount. Since the formation temperature remains the same compared to the base case and has the same potential of heat transfer, a drilling fluid on the low end of the simulation range will therefore gain heat from the formation more easily and thus approach the formation temperature. To show this effect more clearly, the results for a specific heat capacity of 2000 J/kg-°C and a flow rate of 500 l/min is given in figure 3-8. Additionally, if the annulus temperature exceeds that of the formation, a drilling fluid with a low specific heat capacity will lose heat more easily to the formation and the temperature difference between the annulus and formation will decline.

Results for the entire range of specific heat capacities with respect to maximum, bottom hole, and outlet temperatures, are presented in figure 3-9. Similar to the results for flow rate, the maximum and bottom hole temperature is highly sensitive to changes in specific heat capacity. The outlet temperature demonstrates little to practically no effect. It varies with only a few degrees from a value of 30 °C, which is because the annulus temperature will approach the initial formation temperature of 30 °C.
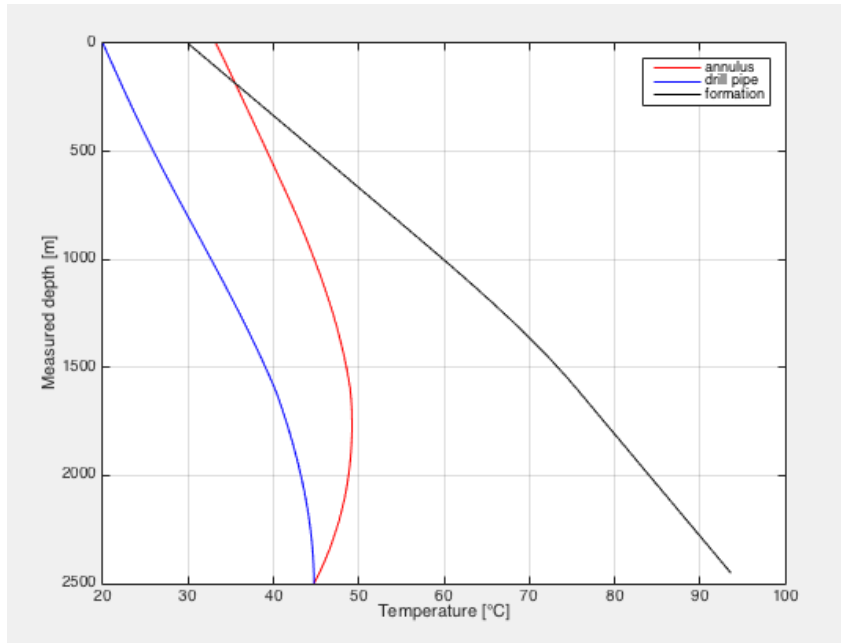
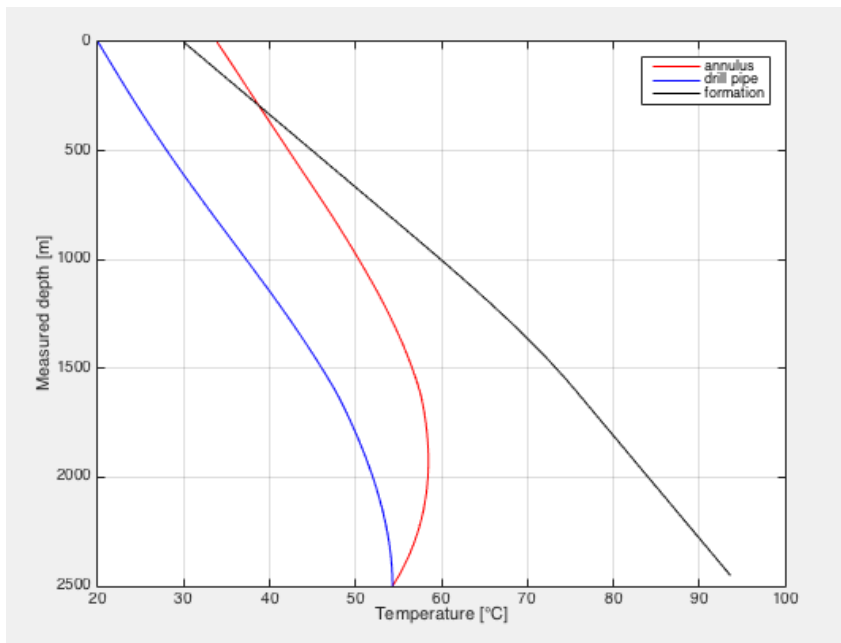*Figure 3-6 Temperature distribution - specific heat capacity: 3000 J/kg-°C*

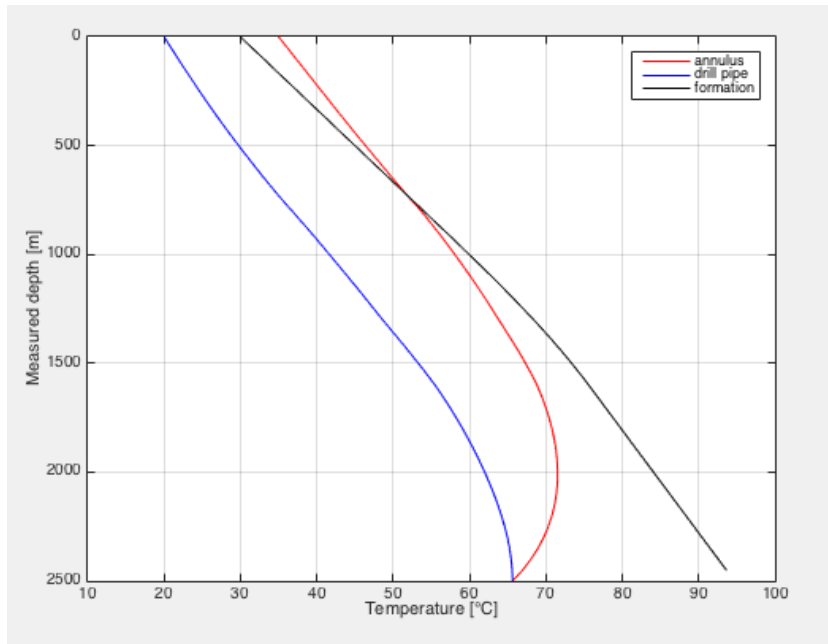*Figure 3-7 Temperature distribution - specific heat capacity: 2000 J/kg-°C*

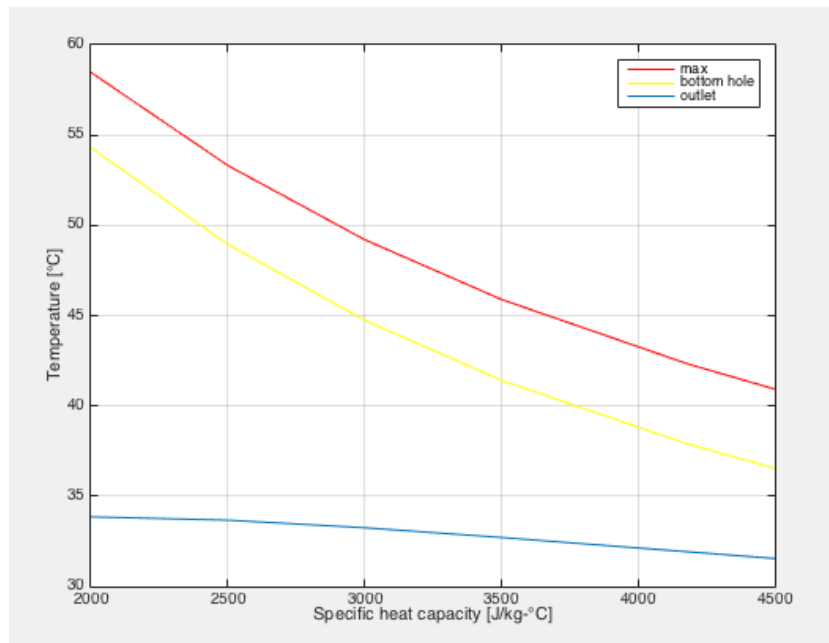*Figure 3-8 Temperature distribution – specific heat capacity: 2000 J/kg-°C, flow rate: 500 l/min*

Figure 3-9 Temperature vs. specific heat capacity

3.5 Thermal conductivity

3.5.1 Drilling fluid

Drilling fluid thermal conductivity is one of the mechanisms of a convective heat transfer process as described in chapter 2.2.1. It affects the CHTC, the overall heat transfer coefficient, and ultimately the rate of heat transfer between the annulus and the drill pipe fluid. Intuitively, increasing the thermal conductivity will decrease the resistance to heat flow and thus increase the rate of heat transfer at the annulus/formation interface and the annulus/drill pipe interface. This is verified by considering the related mathematical expressions given in chapter 2.2.1. A range of thermal conductivity from 0.3 to 0.9 W/m-°C have been considered in the simulations. The base case value of 0.6 W/m-°C represents water. In general, water has a lower thermal conductivity than solids, but higher than gas and oil. The selected range will therefore account for any low conductivity OBM and drilling fluids with high solids content.

The results for thermal conductivities of 0.4 and 0.8 W/m-°C are presented in figures 3-10 and 3-11. For the first case, a decrease of temperatures is seen compared to the base case. An increase of temperatures is found in the results with a conductivity of 0.8 W/m-°C. For example, the difference between the maximum temperature of the base case and the case with 0.9 W/m-°C is about 6%. This indicates that the drilling fluid thermal conductivity makes a difference, but not as pronounced as the flow rate effects. Consequently, the energy transfer by the bulk motion of the fluid is what dominates the overall convective heat transfer in the wellbore. The results for the entire range of considered thermal conductivity values are presented in figure 3-12.
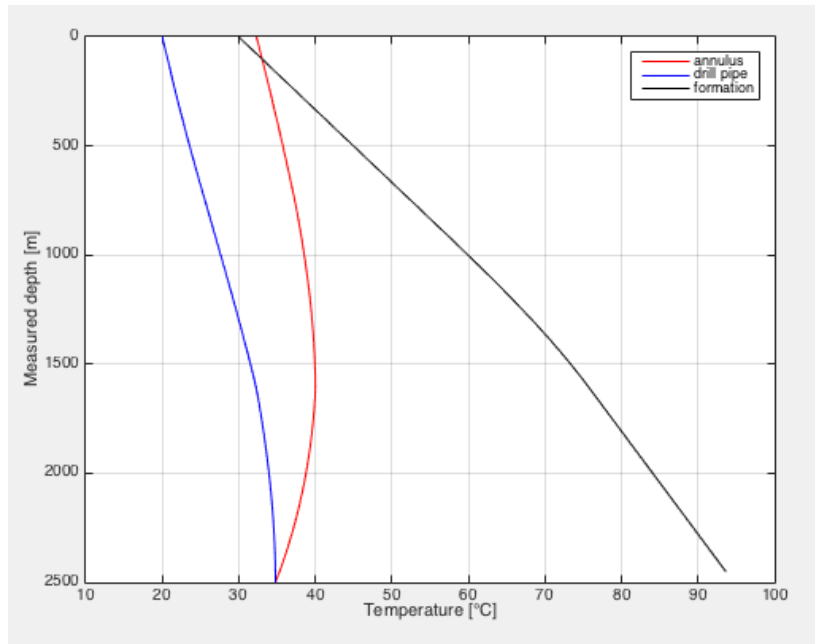
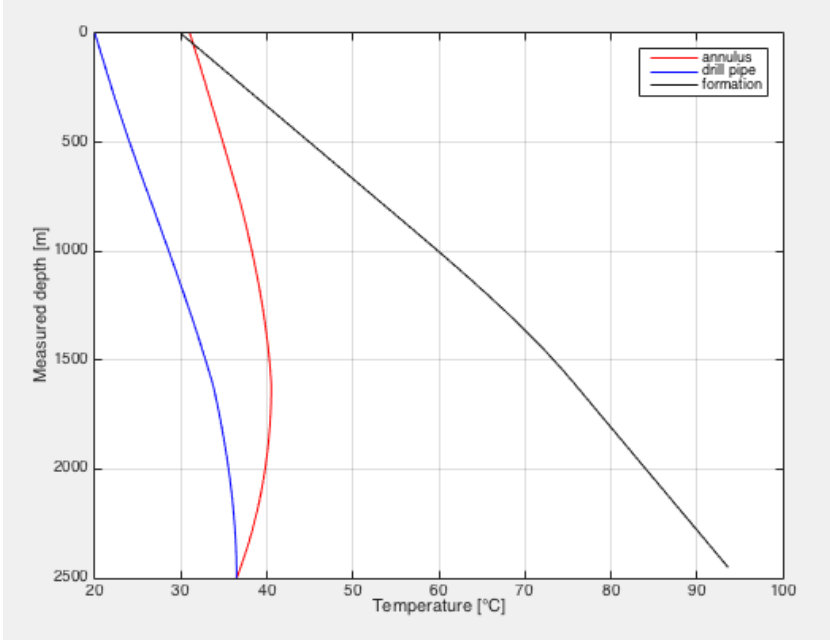*Figure 3-10 Temperature distribution - thermal conductivity: 0.4 W/m-°C*
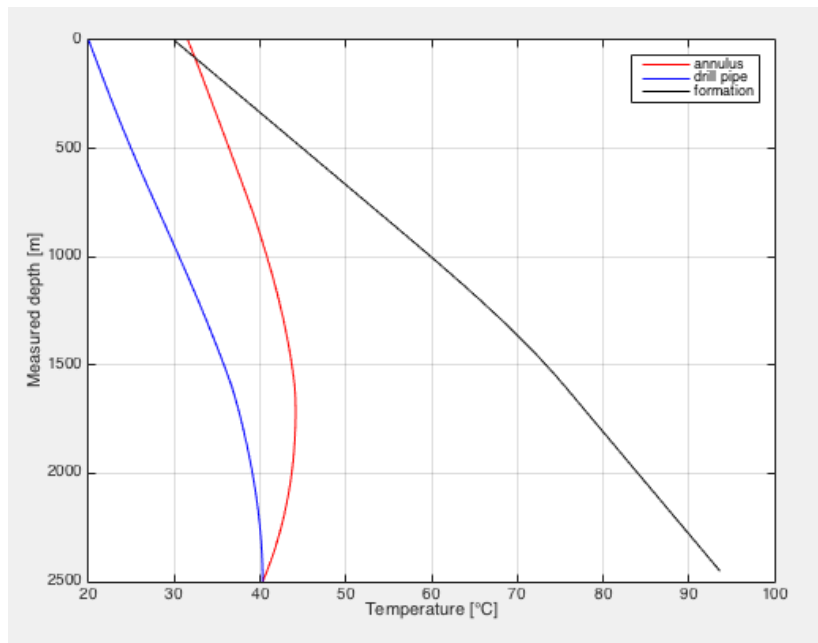
Figure 3-11 Temperature distribution - thermal conductivity: 0.8 W/m-°C
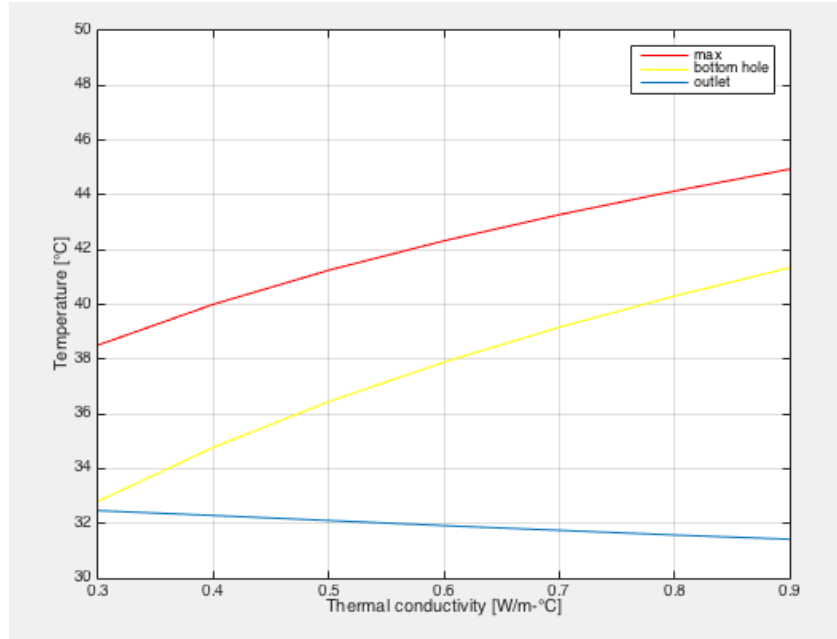
Figure 3-12 Temperature vs. drilling fluid thermal conductivity

3.5.2 Formation

The thermal conductivity of the formation will affect the heat transfer process at the annulus/formation interface. Looking at equation (2.76) reveals that an increase of formation thermal conductivity will increase the rate of heat transfer across the interface.

$$Q_f = \frac{2\pi k_f}{T_D}\left(T_f - T_w\right)dx \qquad (2.76)$$

The simulation results include thermal conductivities in the range of 1.75 to 3.5 W/m-°C. This will include values of conductivity for sandstones at about 1.7 W/m-°C to pure quartz minerals at approximately 3 W/m-°C. Without field data, it is hard to give a proper guess and the base case value is therefore in between the given range. Note that in the base case, an 8.5-in open hole section is considered and the effect of conduction through any layers of casing or cement is consequently not included here.

Results of the simulations are given in figures 3-13 to 3-15. Figure 3-13 represents the results with a formation conductivity of 1.75 W/m-°C. Compared to the base case, the reduction of thermal conductivity has not produced any significant changes. A reduction of the maximum temperature at about 2 °C was found. Increasing the thermal conductivity from the base case value of 2.25 W/m-°C to 3 W/m-°C increased the maximum temperature with approximately

57

7%. The temperature distribution is shown in figure 3-14. Formation thermal conductivity does have an impact on the wellbore temperature distribution and a proper estimation of the parameter is therefore important, but it will not produce the large effects as seen with flow rate and specific heat capacity. At last, Figure 3-15 gives the summary of the considered simulation range.

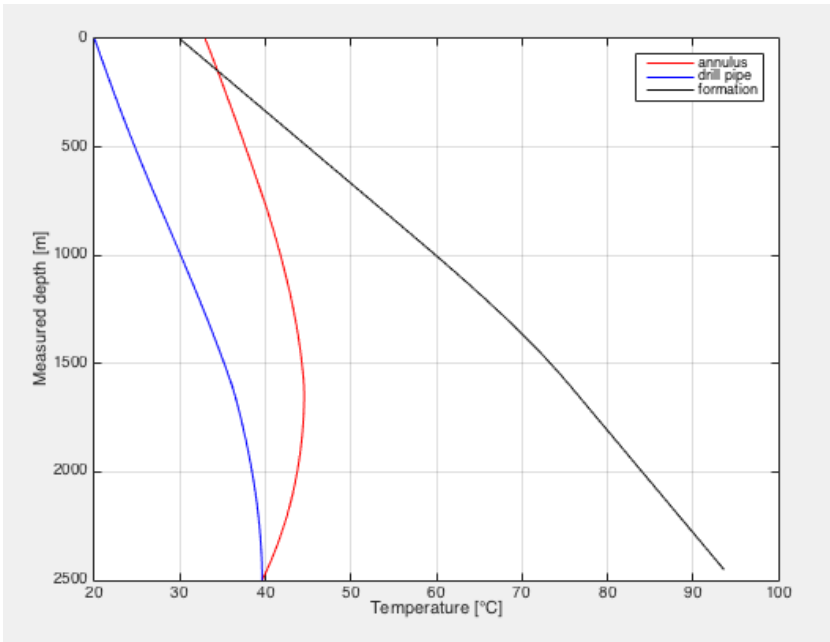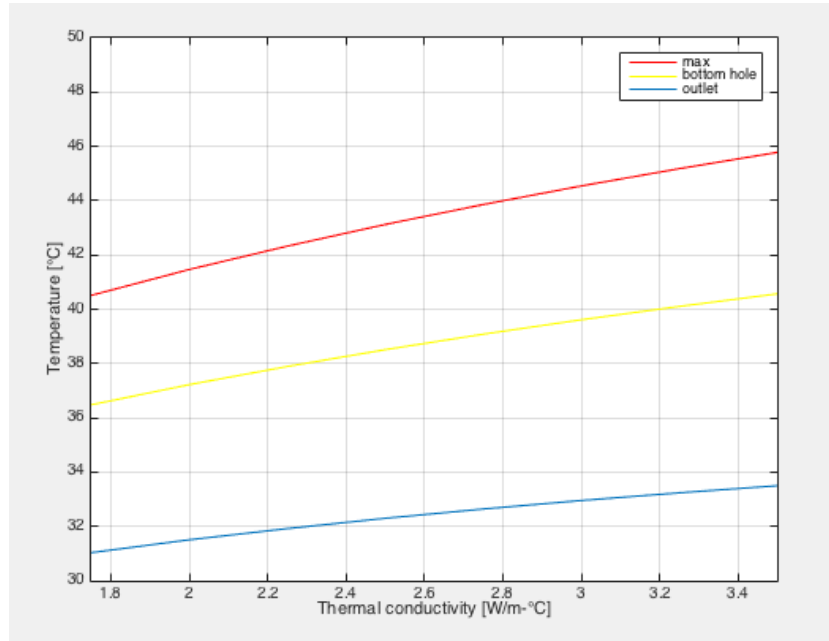*Figure 3-13 Temperature distribution – formation thermal conductivity: 1.75 W/m-°C*

Figure 3-14 Temperature distribution – formation thermal conductivity: 3 W/m-°C

Figure 3-15 Temperature vs. formation thermal conductivity

3.5.3 Drill pipe

The drill pipe thermal conductivity impacts the rate of conductive heat transfer across the drill pipe wall. For example, a drill pipe with a low thermal conductivity will act as a thermal insulator and restrict the heat transfer between the annulus and the drill pipe fluid, leading to a large temperature gradient over the wall. The effect of drill pipe thermal conductivity on the wellbore temperature distribution acts according to the expression for the overall heat transfer given by equation (2.6). Increasing the thermal conductivity will increase the overall heat transfer and reduce the temperature difference between the annulus and the drill pipe. Results from the simulations may determine to what extent the effect is present. The simulations presented in this thesis are performed over a range of 20 to 80 W/m-°C. As an example, stainless steel has a value of 16 W/m-k and chromium 94 W/m-°C. The base case value is 50 W/m-k, which is similar to carbon steel.

Figures 3-16 to 3-18 give the simulation results. The effect of drill pipe thermal conductivity is as expected. Increasing the thermal conductivity leads to less difference between the annulus and the drill pipe temperatures. However, the effect is minimal and it can be neglected. Recording the difference between the annulus and the drill pipe temperature for every box in the wellbore at a thermal conductivity of 30 W/m-°C and taking an average of the differences gives an average value of 13.65 °C. The same procedure for 80 W/m-°C gives an average difference of 13.55 °C, which implies that the thermal drill pipe thermal conductivity produces

no effect on the rate of heat transfer between the annulus and the drill pipe. The wellbore temperature distributions for the two cases are given in figures 3-16 and 3-17, and the results for the entire simulation range is presented in figure 3-18. Evidently, variations in the drill pipe thermal conductivity produce practically no effect on the wellbore temperature distribution.
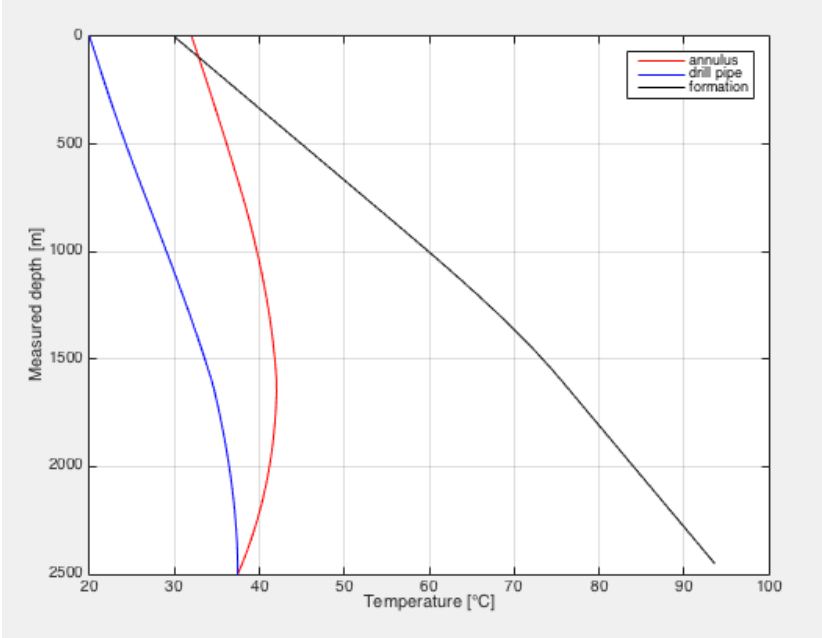

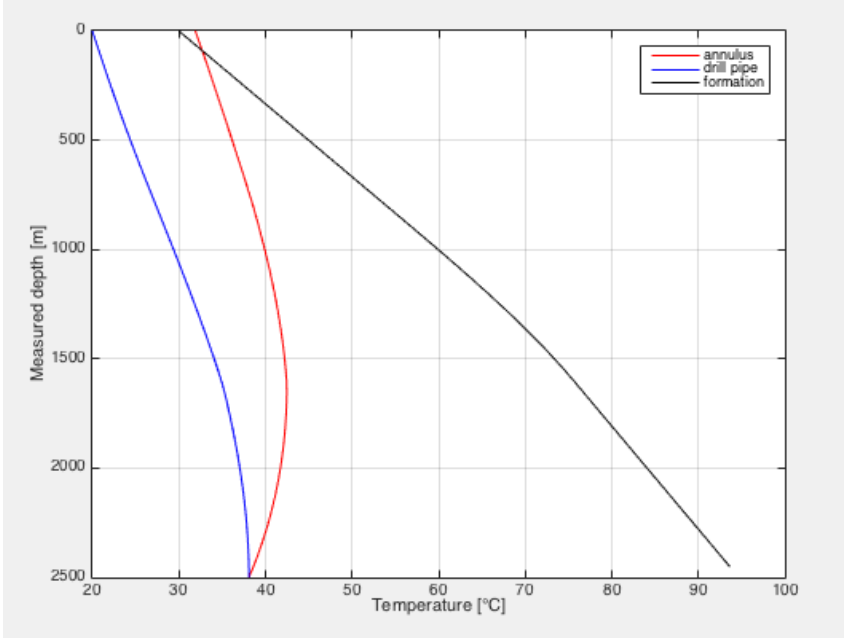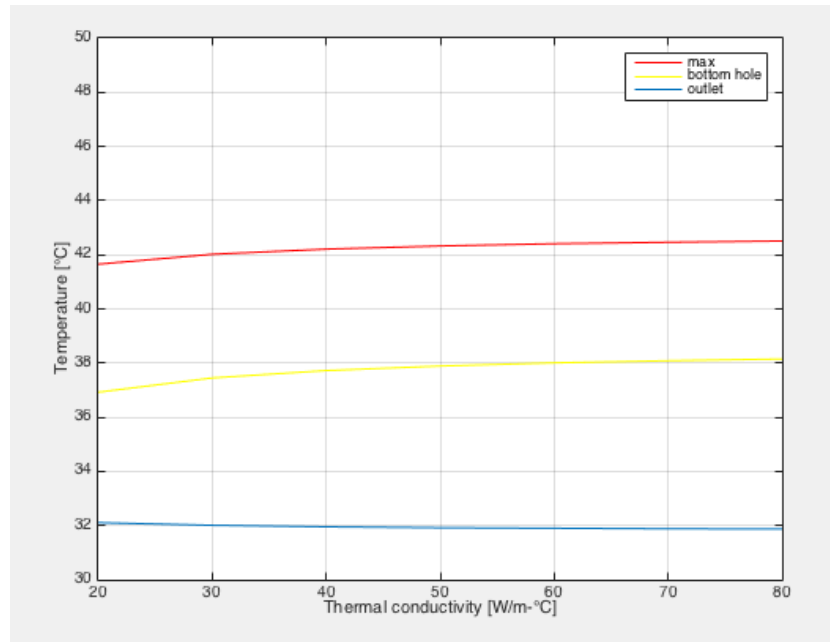*Figure 3-16 Temperature distribution – drill pipe thermal conductivity: 30 W/m-°C*

Figure 3-17 Temperature distribution – drill pipe thermal conductivity: 80 W/m-°C

Figure 3-18 Temperature vs. drill pipe thermal conductivity

3.6 Viscosity

In this work, drilling fluid viscosity is treated as a function of both pressure and temperature. The apparent viscosity is determined by utilizing rheology data from experiments on an OBM as explained in chapter 2.2.3, and the viscosity will thus vary for each box in the wellbore. The viscosity for the base case varies within the range of 30-75 cP. It is hard to determine the exact effect of viscosity on the wellbore temperature distribution when it is changing throughout the wellbore. To make the effect clearer, simulations are performed by assuming a constant viscosity instead. The simulations cover a range of viscosity from 1 cP to 100 cP. Results are presented in figures 3-19 to 3-21.

At first sight, it is obvious that decreasing the viscosity will increase the bottom hole temperature and result in a larger temperature gradient. Decreasing the viscosity from 100 cP to 1 cP gives a 58% increase of bottom hole temperature. The effect of viscosity on the wellbore heat transfer is included in equation (2.13) and the calculation of the CHTC. A low viscosity results in a large CHTC and ultimately an efficient overall heat transfer rate from the formation to the wellbore system. It is therefore crucial to include the non-Newtonian viscosity behavior of drilling fluids. Simplifying calculations by using a Newtonian viscosity model for drilling fluids leads to lower viscosity values and consequently an overestimation of the CHTC and the maximum temperatures in the wellbore.

Another effect of decreasing viscosity is the reduction of difference between the temperatures in the drill pipe and the annulus. The trend is seen by comparing figures 3-19 and 3-20. The results of figure 3-20 with a viscosity of 1 cP show that the temperatures of the drill pipe and the annulus fluids are much closer than in figure 3-19. A decrease of viscosity leads to an increase of the CHTC and ultimately a larger heat transfer rate between the annulus and the drill pipe fluids according to equation (2.6). As the heat transfer increases, the differences in temperature will diminish and the results obtained in figure 3-20 will occur. Also, inspecting the mentioned figures reveals that maximum temperature in the wellbore occurs further down in the wellbore when the viscosity is decreased. This is a consequence of the increased heat flow between the annulus and the drill pipe. As the drill pipe fluid becomes warmer, the bottom hole temperature will increase due to the boundary condition $T_p = T_a$ and approach the maximum temperature.

The results of the full range of viscosities are presented in figure 3-21. These results indicate the effect of the viscosity is more pronounced at the low end of the range. In fact, the effect fades with increasing viscosity. The statement that the maximum temperature in the wellbore moves further down with decreasing viscosity is also obvious in this figure as the bottom hole and maximum temperature approach each other for lower viscosities. An interesting observation is that the outlet temperature decreases with decreasing viscosities, which is the opposite effect of the bottom hole temperature. The increased heat transfer rate will move the outlet temperature towards the drill pipe inlet temperature of 20 °C.
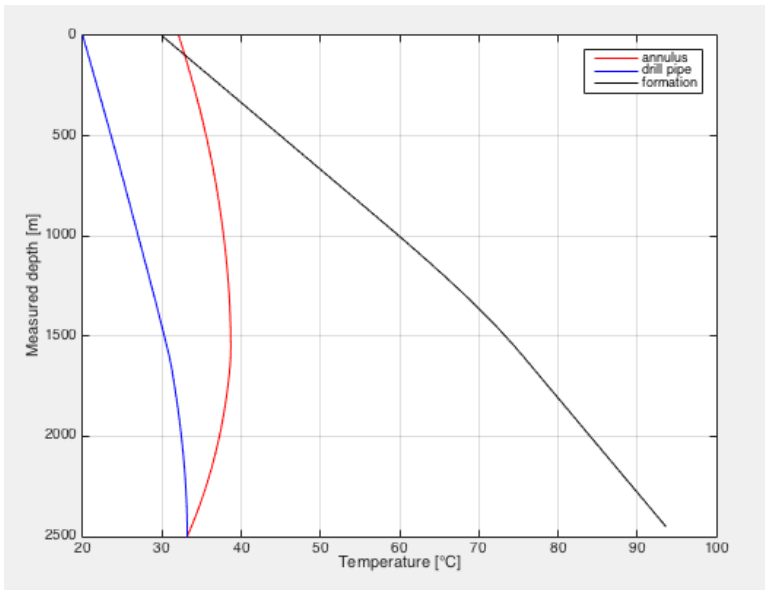

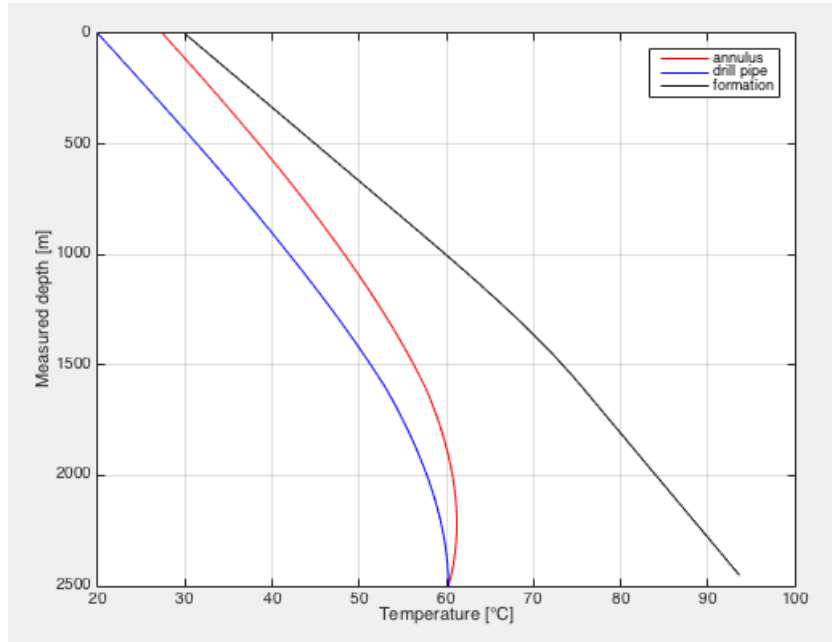*Figure 3-19 Temperature distribution – viscosity: 100 cP*

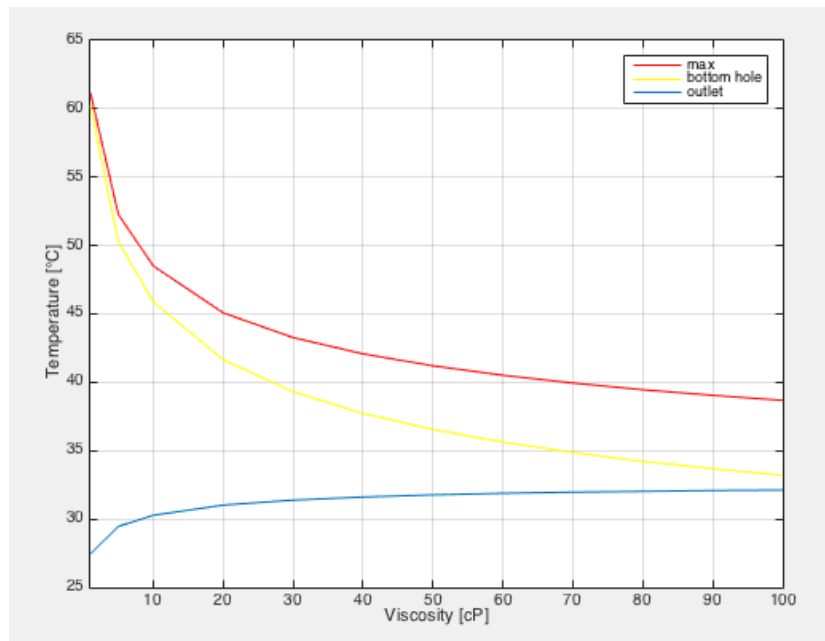*Figure 3-20 Temperature distribution – viscosity: 1 cP*

Figure 3-21 Temperature vs. viscosity

3.7 Drilling fluid density

The density model employed in this thesis is based on an OBM with a reference point of 1205 kg/m^3 at ambient conditions. The fluid behavior with respect to pressure and temperature has been established through a PVT analysis. To determine the effect of drilling fluid density on the temperature distribution, the reference point is varied over a range of 1000-1900 kg/m^3. Figures 3-22 and 3-23 give the results for drilling fluids with a density of 1000 and 1700 kg/m^3 respectively. Increasing the density results in an overall reduction of wellbore temperature. Comparing the maximum temperature of the base case with the results of 1700 kg/m^3 gives a reduction of 14%. The effect is much like the one experienced with flow rate, but less significant. Increasing the density will increase the mass flow rate. This results in a larger heat transfer rate over an annulus element according to equation (2.75). Therefore, the heat that is introduced to the system will also leave the system faster and thus leaving less impact on the temperatures in the system. Figure 3-24 shows the variation in temperatures with density over the entire simulation range. It is obvious that drilling fluid density has a noticeable effect on the wellbore temperature distribution.
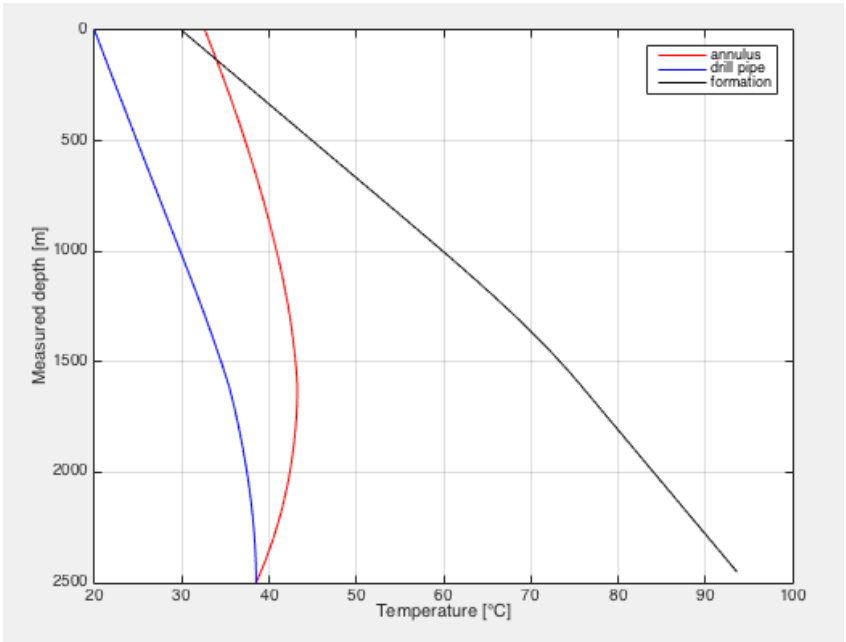

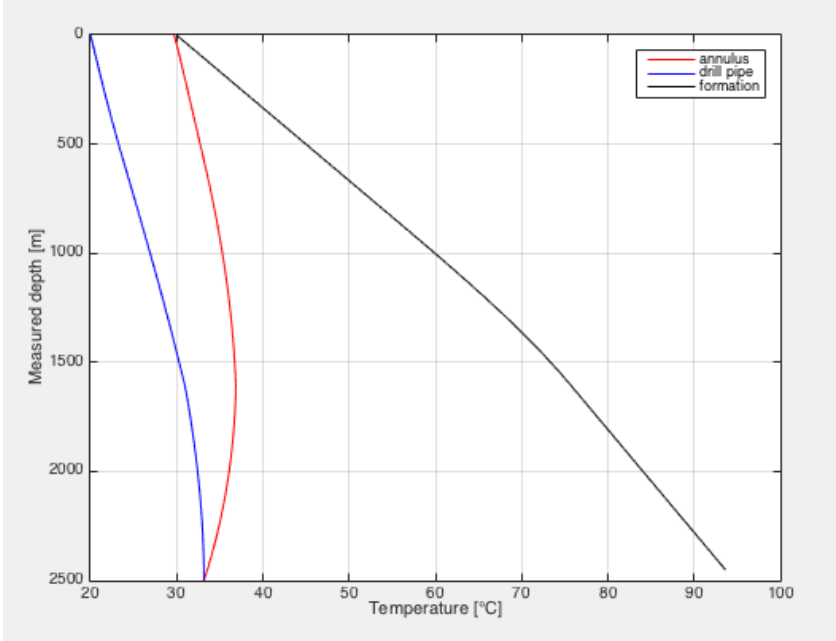*Figure 3-22 Temperature distribution – density: 1000 kg/m^3*

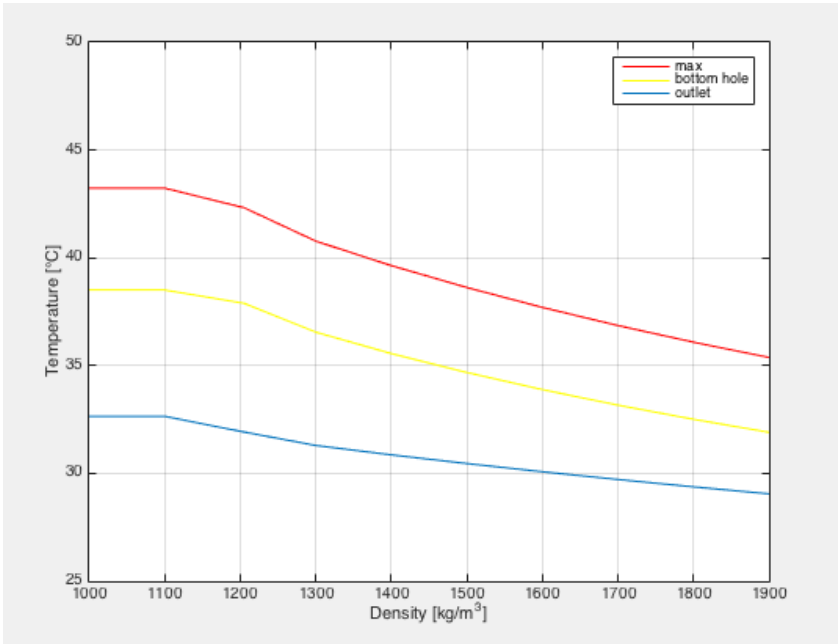*Figure 3-23 Temperature distribution – density: 1700 kg/m³*

Figure 3-24 Temperature vs. drilling fluid density

65

3.8 Geothermal gradient

The geothermal gradient represents the rate of increase in formation temperature with depth. The amount of heat flow from the formation to the annulus is governed by the temperature difference between them. A larger temperature difference results in an increased rate of heat transfer as expressed by equation (2.78). Consequently, changes in the geothermal gradient will affect the rate of heat transfer from the formation and thus the wellbore temperature distribution. Simulations are performed for geothermal gradients in the range of 20-45 °C/km to evaluate the impact. Results are presented by figures 3-25 to 3-27.

Inspecting figures 3-25 and 3-26 reveals that the overall temperature distribution increases with increasing geothermal gradients. Also, note how the maximum formation temperature increases from about 70 °C in figure 3-25 to over 110 °C in figure 3-26. Compared to the base case with a value of 30 °C/km, decreasing the geothermal gradient by 10 °C/km results in a reduction of the maximum wellbore temperature by approximately 17%. Increasing the gradient by 10 °C/km results in an increase of maximum temperature by 15% as illustrated in figure 3-26. This indicates a nearly linear trend between the geothermal gradient and the maximum temperature. Figure 3-27 verifies this statement and that the trend is also representative for the bottom hole and the outlet temperature. Another observation from figure 3-27 is that the slopes of each curve reveal that the maximum temperature is most sensitive to the geothermal gradient, followed by the bottom hole temperature and finally the outlet temperature.
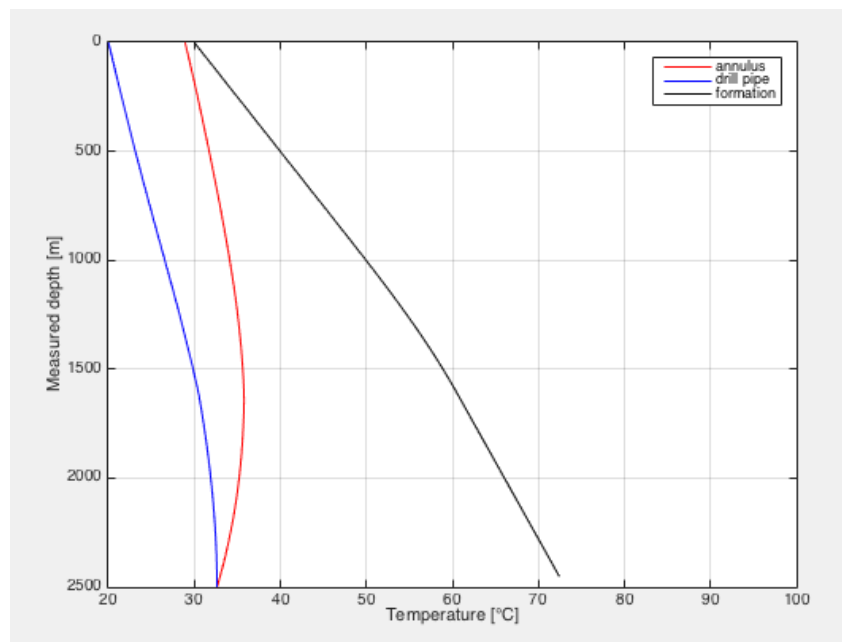

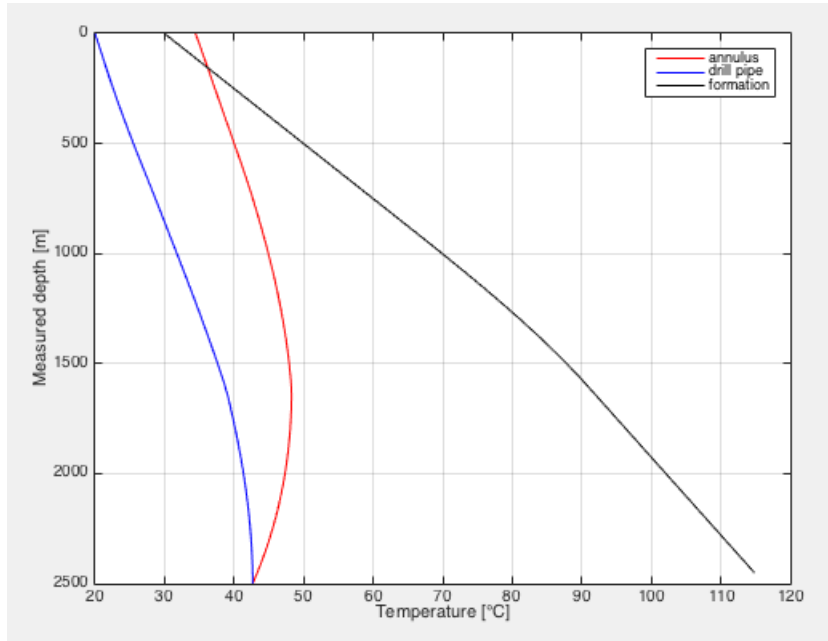*Figure 3-25 Temperature distribution – geothermal gradient: 20 °C/km*

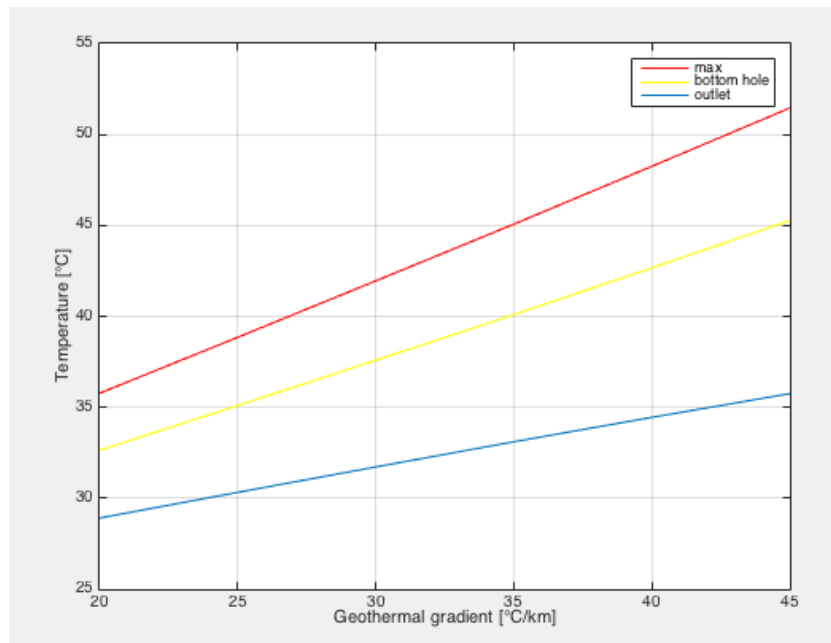*Figure 3-26 Temperature distribution – geothermal gradient: 40 °C/km*

Figure 3-27 Temperature vs. geothermal gradient

3.9 Energy source terms

3.9.1 Joule-Thomson coefficient

The Joule-Thomson coefficient determines the change in drilling fluid temperature with changes in pressure. The wellbore pressure distribution will therefore have a direct impact on the temperature distribution. Varying the flow rate will affect the frictional pressure losses and ultimately the pressure distribution. Therefore, simulations are performed with the same flow rates as in chapter 3.3 and with the effect of the Joule-Thomson coefficient. All the other parameters of the base case remain constant. The depth of the wellbore is also kept constant and the contribution from hydrostatic effects will remain the same. Results are shown in figures 3-28 to 3-29.

Figure 3-28 gives a plot of bottom hole temperature versus flow rate for the base case and a case where the Joule-Thomson coefficient is included. The comparison reveals that the bottom hole temperature decreases when the effect of the Joule-Thomson coefficient is considered. This is because as pressure increases in the drill pipe with flow direction, the drilling fluid compresses and cools according to the discussion in chapter 2.4.4. The reduction in drill pipe temperature will consequently decrease the bottom hole temperature. For the base case flow rate of 1500 l/min, comparing the results without the effect of the Joule-Thomson coefficient and with the effect gives a reduction of bottom hole temperature by 4%. Furthermore, the effect diminishes with increasing flow rate.

A comparison of the outlet temperature with and without the effect of the Joule-Thomson coefficient is given in figure 3-29. The results indicate the opposite effect for the outlet temperature. Including the effect of the Joule-Thomson coefficient increases the outlet temperature compared to the base case and the effect increases with increasing flow rate. Again, according to chapter 2.4.4, the pressure decreases with the flow direction in the annulus and the drilling fluid will expand and become warmer. The increase of outlet temperature for the base case flow rate is by 3%. Consequently, the effect of the Joule-Thomson coefficient will impact the temperature distribution, but it is not a dominating factor for the wellbore temperature distribution.
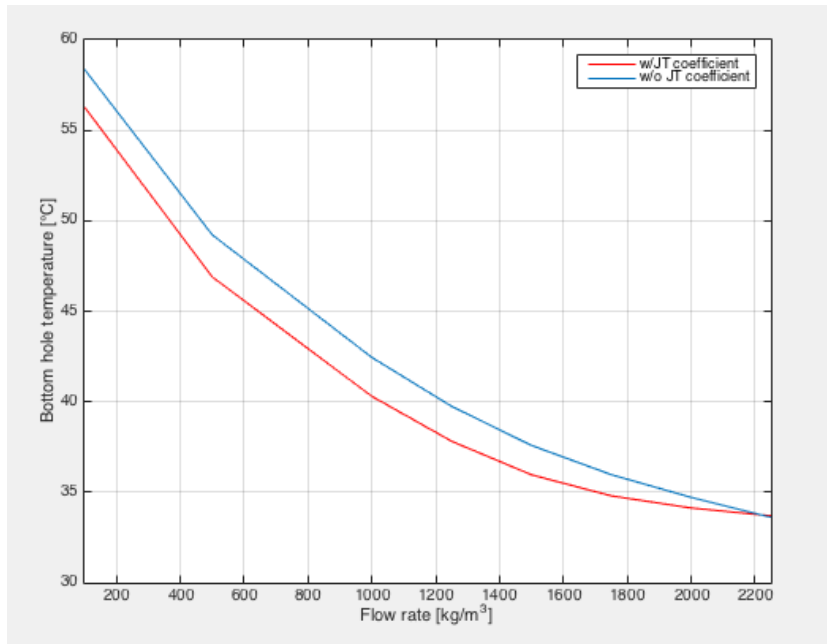
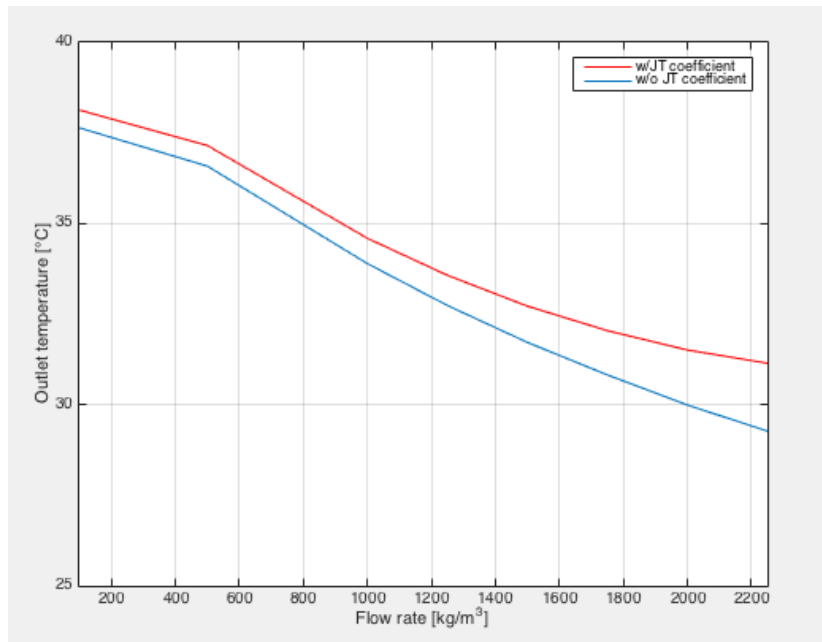*Figure 3-28 Bottom hole temperature vs. flow rate*

Figure 3-29 Outlet temperature vs. flow rate

69

3.9.2 Drill pipe rotation

The amount of heat generation from drill pipe rotation is governed by the wellbore torque and the drill pipe rotational speed as given by equation (2.58). Two critical factors for torque in an ERD well are wellbore inclination and friction. A section with a high inclination gives a large normal force because a large portion of the drill pipe weight will lay on the low side of the wellbore, ultimately leading to significant frictional forces. Also, a high friction factor increases the frictional forces. Therefore, the sensitivity analysis is performed with respect to these two parameters together with the rotational speed of the drill pipe. Note that the torque is calculated by the model of Aadnoy et al. (2010). Some of the most important input parameters of this model and the corresponding values used in this thesis, is given in table 3-2. The wellbore inclination, pipe rotational speed, and friction factor have been varied to obtain the results in figures 3-30 and 3-31.

Figure 3-30 shows the effect of pipe rotation on the temperature distribution. The effect is compared to the base case given in chapter 3.2, only now the base case includes varying wellbore inclination. Maximum temperatures obtained by simulating the effect of pipe rotation are compared to the maximum temperatures of the base case and given in figure 3-30 as a percentage increase. The friction factor used for the simulations shown in figure 3-30 is 0.3. Result reveal that heat generation from pipe rotation is not a contributing factor to the overall temperature distribution. The largest increase of maximum temperature occurs at an inclination of 80 degrees with 150 RPM, yielding a 3% increase. Compared to a handful of the other parameters investigated in chapter 3, these results are insignificant. However, note that the wellbore in the base case is only 2500 meters MD. A longer section will increase the total torque losses and a more pronounced effect might occur. Still, drilling fluid parameters would dominate the temperature distribution.

Even though the drill pipe rotation does not generate a significant amount of heat, the temperature model in this thesis can be used to determine how parameters in the torque model affect the wellbore temperature. For example, in figure 3-31 a friction factor of 0.15 has been used to generate the results. The largest increase of maximum temperature is now less than 1.6%, which is a reduction of almost 50% compared to the largest increase in figure 3-30. Also, it obvious from both figures that increasing the wellbore inclination and RPM will increase the effect of pipe rotation on the temperature distribution. It is also possible to determine the effect of the other parameters given in table 3-2, but since it has been established that pipe rotation

does not generate a significant amount of heat, investigation of other parameters related to the torque model is not a part of the objective in this work.

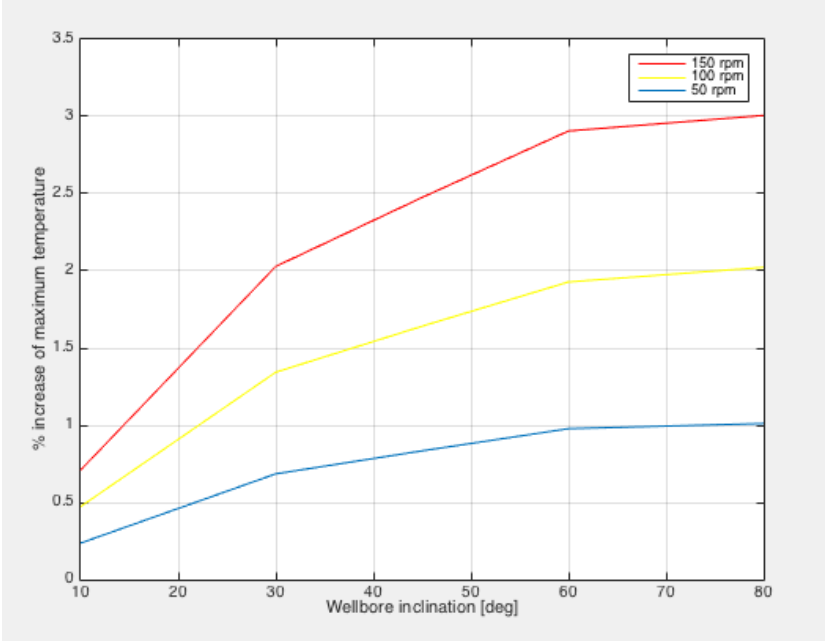|		
Axial speed (ROP)	30	m/hr
RPM	100	1/min
Friction factor	0.3	-
Pipe unit weight	450	N/m
WOB	90	kN
Bit torque	10	kNm

Table 3-2 Torque model parameters

Figure 3-30 Increase in maximum temperature vs. wellbore inclination – friction factor: 0.3
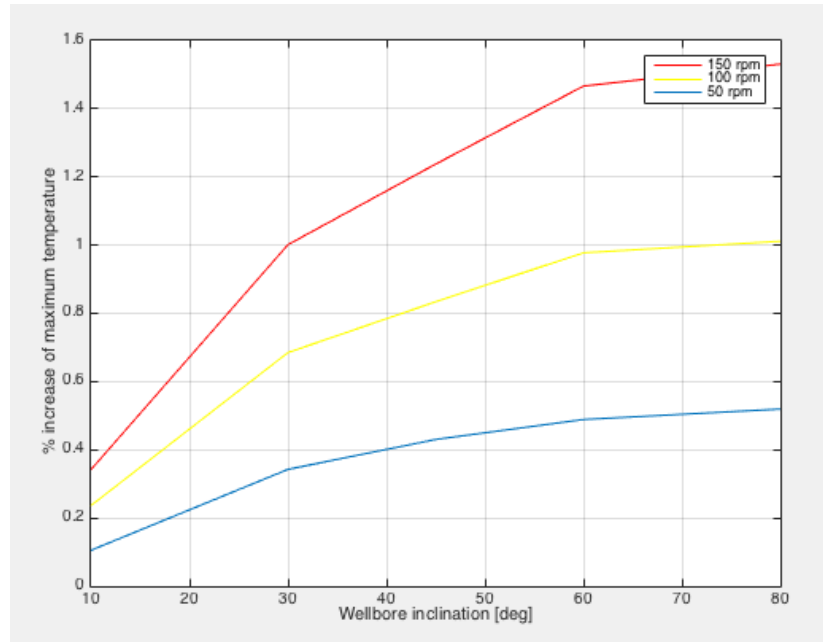
Figure 3-31 Increase in maximum temperature vs. wellbore inclination – friction factor: 0.15

3.9.3 Drill bit friction

Heat generation from drill bit friction is in this thesis related to the effect of pipe rotation. As mentioned in chapter 2.4.2, some authors have suggested that a certain percentage of the total mechanical input used to rotate the drill pipe is spent on overcoming frictional forces between the drill bit and the formation. However, the exact percentage is not a known factor. Simulations are therefore performed with varying percentages to evaluate the effect of bit friction on the temperature distribution. Compared to the heat generation from pipe rotation which is distributed along the wellbore, the heat generation from drill bit friction is only present as a heat source at the bottom of the wellbore. Based on that note, the effects of drill bit friction on the bottom hole temperature is presented in figure 3-32. Furthermore, to include the effect, the total heat generated from pipe rotation only is multiplied with the given percentage and used to represent the amount of heat introduced by the bit.

Figure 3-32 shows a plot of bottom hole temperature versus wellbore inclination. The blue curve represents the bottom hole temperature including the effects of pipe rotation as explained in chapter 3.9.2, but the drill bit friction is not included, hence 0% for the legend. Table 3-2 is used to obtain these results. First, the general observations without the drill bit friction is studied. The trend of the blue curve shows an increase of bottom hole temperature from 10-30

degrees before the bottom hole temperature decreases. Without the effect of pipe rotation at all, bottom hole temperature will decrease with increasing inclination. This is because sections with high inclinations are less deep in terms of TVD and the formation temperature will consequently be lower. On the contrary, including the effect of pipe rotation gives an increase of bottom hole temperature from 10-30 degrees as shown in figure 3-32, indicating that the heat generation from pipe rotation counteracts the effect from reduction of formation temperature. From 30-80 degrees, the effect of lower formation temperatures dominates and the bottom hole temperature decreases.

When the effect of drill bit friction is included, the increase of bottom hole temperature from 10-30 degrees becomes more pronounced as the percentage of mechanical input required to overcome the drill bit friction is increased. This shows that the bit friction influences the temperature distribution. However, it must be emphasized that the effect bit friction impose on the temperature distribution is marginal. At an inclination of 30 degrees, comparing the bottom hole temperature for the 0%-curve to the temperature at the 40%-curve gives an increase of less than 1%.

The effect of drill bit friction on maximum wellbore temperature is shown in figure 3-33. Again, the blue curve represents temperatures with the effect of pipe rotation without including the drill bit friction. It is obvious that the maximum temperature for this curve decreases with increasing wellbore inclinations. As the effect of drill bit friction is included and increased by percentage, it will counteract the effects of reduced formation temperature from 10-30 degrees just as in figure 3-33. Still, the effects of including bit friction are small. Considering results from both figures in this chapter, it is concluded that the effect bit friction impose on the temperature distribution in this work, is negligible.
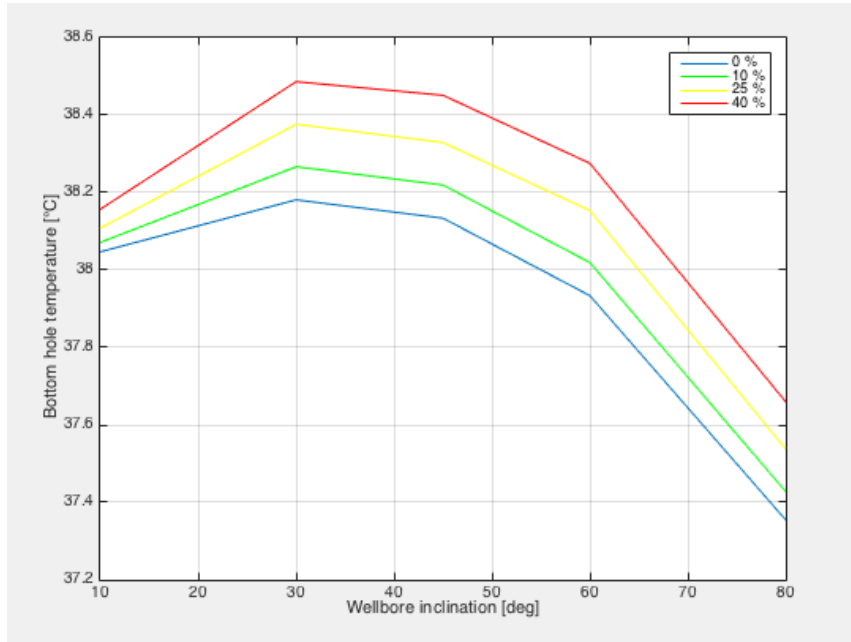
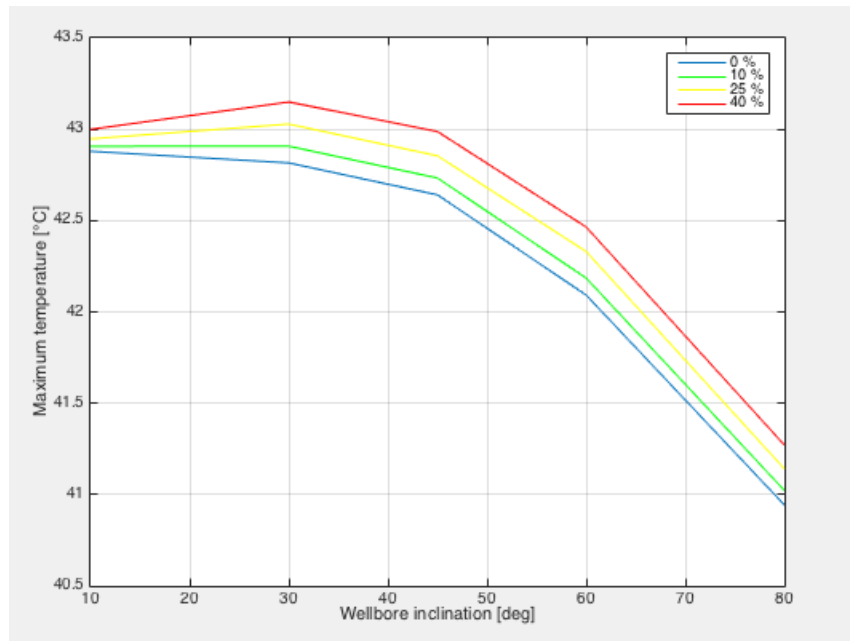*Figure 3-32 Bottom hole temperature vs. wellbore inclination*

Figure 3-33 Maximum temperature vs. wellbore inclination

3.9.4 Frictional pressure losses

As explained in chapter 2.4.3, frictional pressure losses will introduce heat to the wellbore system. The effect of frictional pressure losses on the wellbore temperature distribution is expected to increase with increasing flow rate and correspondingly larger pressure losses. Simulations are performed using the base case with varying flow rates in the range of 100-2250 l/min. The effects of including the frictional pressure losses are compared to the base case results with no source terms.

Figure 3-34 shows the maximum wellbore temperature versus flow rate, where the red curve represents the results including the effect of frictional pressure losses and the blue curve represents the base case results with no source term. Evidently, including heat generation from frictional pressure losses yields little to no effect on the maximum wellbore temperature. Figure 3-35 reveals that the effect is also minimal on the bottom hole temperature. At a flow rate of 2250 l/min where the effect is largest, the bottom hole temperature for the two scenarios differ by only 2%. Thus, heat generation from frictional pressure losses produce a small effect on the wellbore temperature distribution.
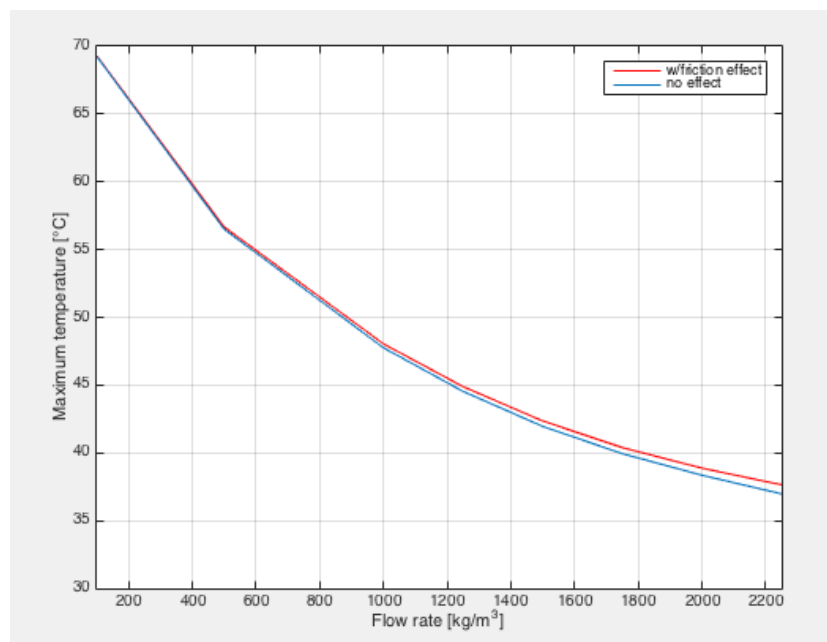

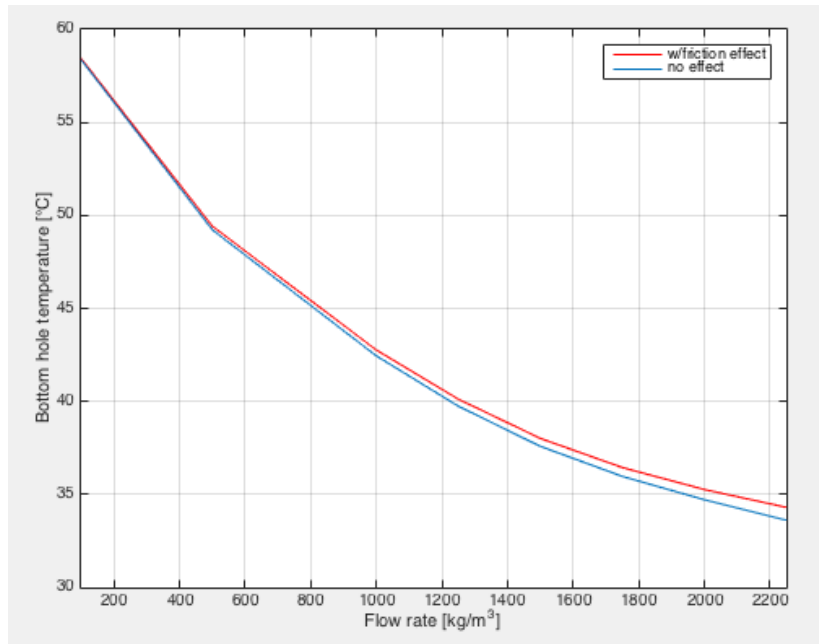*Figure 3-34 Maximum temperature vs. flow rate*

Figure 3-35 Bottom hole temperature vs. flow rate

4 Conclusion

Analyzing the simulation results reveals that flow and drilling fluid properties are the dominant factors for the wellbore temperature distribution. Changes in flow rate are found to have a large effect on the maximum and bottom hole temperatures. Increasing the flow rate results in reduced wellbore temperatures and more even temperature distributions in the drill pipe and the annulus. The same effect but less pronounced, occurs while increasing the drilling fluid density. Moreover, an increase of these two parameters results in a stronger convective heat transfer within the fluid column, which ultimately reduce the impact of the formation temperature on the wellbore temperature distribution.

Another parameter that produce a noticeable impact on the temperature distribution is the drilling fluid specific heat capacity. Results indicate that drilling fluids with a low specific heat capacity tend to have temperatures much closer to the formation temperature. Decreasing the specific heat capacity of the fluid will increase its ability to gain heat and thus increase its temperature. Furthermore, the maximum and bottom hole temperatures are highly sensitive to this parameter. It is therefore critical to have correct estimations of the specific heat capacity to avoid any unforeseen high wellbore temperatures.

Drilling fluid viscosity is also found to be a dominant factor for the temperature distribution. Results from the simulations show that drilling fluids with viscosities close to that of water give significantly higher wellbore temperatures compared to more viscous fluids. A low viscosity fluid yields a higher CHTC and consequently a more efficient heat transfer with the formation. This emphasize that it is important to apply an appropriate model and to ensure accurate estimations of the viscosity. Including the non-Newtonian behavior of drilling fluids to determine the viscosity is therefore of great importance, and the use of viscosity measurements to determine the rheological behavior of the considered OBM in this thesis has provided a more accurate temperature model.

The effects of energy source terms that occur during drilling is also investigated in this work. In general, results show that the overall contribution from these terms is not predominant. For example, the Joule-Thomson coefficient will impact the bottom hole pressure but to a much less extent than the flow rate or the viscosity. Heat generation due to friction is also found to produce little to no effect on the temperature distribution. However, considering a wellbore

with a longer horizontal section might give a more pronounced impact. From another perspective, including heat generation due to frictional forces offers the ability to determine how wellbore design and operational parameters such as RPM and WOB impact the temperature distribution. Also, considering energy source terms will improve the accuracy of the temperature model and it is suggested that they are not neglected. After all, ERD wells may encounter conditions where only a small increase of temperature makes a difference.

References

Alves, I. N., Alhanati, F. J. S., & Shoham, O. (1992). A Unified Model for Predicting Flowing Temperature Distribution in Wellbores and Pipelines. doi:10.2118/20632-PA

Bergman, T. L., Incropera, F. P., DeWitt, D. P., & Lavine, A. S. (2011). *Fundamentals of heat and mass transfer*: John Wiley & Sons.

Bhushan, B. (2000). *Modern tribology handbook, two volume set*: CRC press.

Cameron, C. (2001). *Drilling Fluids Design and Management for Extended Reach Drilling*.

Chiu, K., & Thakur, S. C. (1991). *Modeling of Wellbore Heat Losses in Directional Wells Under Changing Injection Conditions*.

Corre, B., Eymard, R., & Guenot, A. (1984). *Numerical Computation of Temperature Distribution in a Wellbore While Drilling*.

Fan, H., Zhou, H., Wang, G., Peng, Q., & Wang, Y. (2014). *Utility Hydraulic Calculation Model of Herschel-Bulkley Rheological Model for MPD Hydraulics*.

Forrest, J., Marcucci, E., & Scott, P. (2005). Geothermal gradients and subsurface temperatures in the northern Gulf of Mexico.

Hamrick, T. R. (2011). *Optimization of Operating Parameters for Minimum Mechanical Specific Energy in Drilling*: West Virginia University.

Hasan, A. R., & Kabir, C. S. (1991). *Heat Transfer During Two-Phase Flow in Wellbores; Part I--Formation Temperature*.

Holmes, C. S., & Swift, S. C. (1970). Calculation of Circulating Mud Temperatures. doi:10.2118/2318-PA

Kabir, C. S., Hasan, A. R., Kouba, G. E., & Ameen, M. (1996). Determining Circulating Fluid Temperature in Drilling, Workover, and Well Control Operations. doi:10.2118/24581-PA

Keller, H. H., Couch, E. J., & Berry, P. M. (1973). Temperature Distribution in Circulating Mud Columns. doi:10.2118/3605-PA

Kumar, A., & Samuel, R. (2013). Analytical Model To Predict the Effect of Pipe Friction on Downhole Fluid Temperatures. doi:10.2118/165934-PA

Maghari, A., & Safaei, Z. (2007). Predictions of the Joule-Thomson Inversion Curve for Water and Methanol from the LJ-SAFT EOS. *Iranian Journal of Chemistry and Chemical Engineering (IJCCE), 26*(4), 69-74.

Marshall, D. W., & Bentsen, R. G. (1982). A Computer Model to Determine the Temperature Distributions In a Wellbore. doi:10.2118/82-01-05

Metzner, A. B., & Reed, J. C. (1955). Flow of non-newtonian fluids—correlation of the laminar, transition, and turbulent-flow regions. *AIChE Journal, 1*(4), 434-440. doi:10.1002/aic.690010409

Moore, P. L. (1974). Pressure Losses in the Circulating System (1974 DPM Chapter 7): Society of Petroleum Engineers.

Munson, B. R., Young, D. F., & Okiishi, T. H. (2006). *Fundamentals of fluid mechanics* (5th ed. ed.). Hoboken, N.J: Wiley.

Payne, M. L., Cocking, D. A., & Hatch, A. J. (1994). *Critical Technologies for Success in Extended Reach Drilling*.

Poling, B. E., Prausnitz, J. M., & O'connell, J. P. (2001). *The properties of gases and liquids* (Vol. 5): Mcgraw-hill New York.

Ramey, H. J., Jr. (1962). Wellbore Heat Transmission. doi:10.2118/96-PA

Raymond, L. R. (1969). Temperature Distribution in a Circulating Drilling Fluid. doi:10.2118/2320-PA

Reed, T. D., & Pilehvari, A. A. (1993). *A New Model for Laminar, Transitional, and Turbulent Flow of Drilling Muds*.

Rohsenow, W. M., Hartnett, J. P., & Cho, Y. I. (1998). *Handbook of heat transfer* (Vol. 3): McGraw-Hill New York.

Rubiandini R.S, R. (2008). *Extended Reach Drilling (ERD) Design in Deepwater Application*.

Santoyo, E., Garcia, A., Espinosa, G., Santoyo-Gutiérrez, S., & González-Partida, E. (2003). Convective heat-transfer coefficients of non-Newtonian geothermaldrilling fluids. *Journal of Geochemical Exploration, 78*, 249-255. doi:http://dx.doi.org/10.1016/S0375-6742(03)00146-8

Santoyo-Gutiérrez, E. R. (1997). *Transient numerical study simulation of heat transfer processes during drilling of gheothermal wells.* (Ph.D), University of Salford, Salford, UK.

Schroeder, D. V. (2000). *An introduction to thermal physics*: San Francisco, CA : Addison Wesley, [2000] ©2000.

Stamnes, Ø. N. (2011). *Nonlinear estimation with applications to drilling.* Skipnes.

Thompson, M., & Burgess, T. M. (1985). *The Prediction of Interpretation of Downhole Mud Temperature While Drilling*.

Tomren, P. H., Iyoho, A. W., & Azar, J. J. (1986). Experimental Study of Cuttings Transport in Directional Wells. doi:10.2118/12123-PA

Warren, T. M. (1989). Evaluation of Jet-Bit Pressure Losses. doi:10.2118/17916-PA

Aadnoy, B. S., Fazaelizadeh, M., & Hareland, G. (2010). A 3D Analytical Model for Wellbore Friction. *Journal of Canadian Petroleum Technology, 49*(10), 25-36.

Aadnøy, B. S. (2010). *Modern well design* (2 ed.). Boca Raton: CRC Press/Balkerna.